Sorption interactions and behavior of bentonite-lignite based composite toward immobilization of dyes, pharmaceuticals and surfactants

Agnieszka Solińska [a,*], Tomasz Bajda [a], Mariusz Gackowski [b]

[a] *AGH University of Krakow, Faculty of Geology, Geophysics and Environmental Protection, Al. A. Mickiewicza 30, 30-059, Krakow, Poland*
[b] *Jerzy Haber Institute of Catalysis and Surface Chemistry Polish Academy of Sciences, Niezapominajek 8, 30-239, Krakow, Poland*

ARTICLE INFO

ABSTRACT

The presence of dyes, pharmaceuticals, and surfactants in the environment results from extensive industrial and societal progress, prompting the need to explore efficient and safe techniques for their removal. Common concentrations in wastewater can range from micrograms to milligrams per liter, which is concerning due to their persistence and potential health impacts. The sustainable approach of using a nonconventional, eco-friendly mineral-organic composite might address this environmental issue. This study focuses on utilizing a composite of bentonite (BEN) and lignite (LIG) as a sorbent for dyes: Rhodamine b (RB), Remazol brilliant blue r (RBBR), pharmaceuticals: ibuprofen (IB), sulfamethoxazole (STX), and surfactant: sodium dodecylbenzenesulfonate (SDBS) from both synthetic solutions and real wastewater. BEN was chosen for its high cation exchange capacity, while LIG was selected for its ability to adsorb both anionic and cationic formsdiverse functional groups. The composite with BEN to LIG ratio of 20:80 (BL 20:80) demonstrated superior sorption capacity. The adsorption performance is quantified, showing removal efficiencies of up to 18.9 mg RBBR/g, 22.8 mg RB/g, 1.77 mg IB/g, 1.47 mg STX/g, and 4.7 mg SDBS/g. Sorption efficiency is influenced by factors such as the initial sorbate concentration, the pH of the solution, the form of sorbates, and the adsorbents textural, physicochemical (point of zero charge pH_{ZPC}), ion-exchange capacity, hydrophobicity/hydrophilicity) properties. Generally, STX and RB is favored by slightly acidic conditions (pH 4–7), while RBBR and IB are favored by alkaline conditions (pH > 7). The complex physical sorption mechanism includes hydrogen bonding, electrostatic and dispersion forces, as well as π-π interactions. Nuclear magnetic resonance spectroscopy (NMR) suggests that a significant portion of the hydrogen bonding interactions contributes to RB adsorption. The sorption results indicate that the specially-designed mineral composite can effectively remove various chemically distinct organic compounds from real wastewater. Subsequent investigations will focus on the granulated BL 20:80 composite and its applicability in dynamic column systems. This aligns with the ongoing development of purification technologies.

1. Introduction

It is estimated that of the approximately 360 km³/year of global domestic and municipal wastewater production, 190 km³/year are treated in wastewater treatment plants, whereas ~170 km³/year is discharged directly into the environment (Jones et al., 2021). A concerning issue is the growing amount of organic contaminants in wastewater. Conventional wastewater treatment facilities are ineffective in removing micropollutants, such as caffeine, bisphenol A, 4-nonylphenol, and technical 4-nonylphenol, along with various other organic components (Anliker et al., 2020; Belete et al., 2023; Burzio et al., 2022; Clara et al., 2011; Isik et al., 2022; Klamerth et al., 2012; Moretti et al., 2024;

Pathak et al., 2020; Perkins et al., 2017). Contaminants like pharmaceuticals, dyes, and surfactants, present in the water discharged from wastewater treatment plants into rivers, can permeate the environment. This poses a significant risk to aquatic organisms and human health, represent a crucial global problem. Pharmaceuticals are present as compounds and their metabolites in surface and groundwater. The presence of antibiotics in the water is concerning, as it can contribute to the development of antibiotic resistance in pathogens (Kumar et al., 2019; Yuan et al., 2023). Surfactants used in industry (such as detergents, cosmetics, and textiles) and dyes found in wastewater (Arora et al., 2022; Badmus et al., 2021; Johnson et al., 2021; Palmer and Hatley, 2018) have toxic properties. Dyes are particularly resistant to

---

* Corresponding author.
  E-mail address: asolinska@agh.edu.pl (A. Solińska).

degradation and can remain in the aquatic environment for long periods. Surfactants complicate both wastewater treatment and pretreatment by causing the dissolution of hazardous organic micropollutants, pesticides, and polycyclic aromatic hydrocarbons (Kietzmann, 1993; Linclau et al., 2016).

Various methods are used to remove pharmaceuticals from water and wastewater, such as activated sludge systems (Katare et al., 2023; Mantovani et al., 2024), membrane bioreactors (Hai and Price, 2021; Johnson et al., 2024), electrocoagulation (Ammar et al., 2023; Mao et al., 2023), magnetic ion exchange resins (Devaisy et al., 2023; Tamanna et al., 2023), oxidation processes (Zawadzki, 2022) and adsorption - the latter being the most effective for drug removal (Akhtar et al., 2016; Mansouri et al., 2021). The physicochemical and biological techniques for dye removal are used (Donkadokula et al., 2020; Kausar et al., 2018). Chemical methods (e.g., photolysis and photocatalytic processes), biological methods (e.g., anaerobic and aerobic degradation), and physiochemical methods (e.g., electro-kinetic coagulation, ion exchange, adsorption, and membrane filtration), are also utilized to remove dyes from wastewater. All these methods have limitations in cost, design, and dye separation efficiency. Adsorption is the most suitable method compared with the others (Ehsan et al., 2017; Vinayagam et al., 2022). The removal of surfactants from aqueous solutions has been studied for several decades. Numerous studies on removing ionic and non-ionic surfactants have demonstrated that adsorption methods hold the most promise (Amirianshoja et al., 2013; Dikmen et al., 2020; Rezazadeh et al., 2023; Shreya et al., 2021). One of the most popular adsorbents is activated carbon, but it has a relatively high cost and a complicated regeneration process (Santos et al., 2022; Styszko et al., 2015). This has prompted the search for alternative, low-cost adsorbents for the removal a wide variety of organic contaminants from water.

While many papers describe the effectiveness of mineral and organic sorbents for removing organic pollutants (Berhane et al., 2017; Ewis et al., 2022; Gil et al., 2021; He et al., 2021; Ighalo et al., 2022; Karić et al., 2022; Lan et al., 2022; Li and Wei, 2022; Wang et al., 2017; Wen et al., 2020; Wu et al., 2020; Zhao et al., 2023), the data on sorption mechanisms are sparsely described. Published articles provide selective, unrelated data on the effects of pH and initial concentration of sorbates, hydrophilic/hydrophobic interactions, ionic interaction, physisorption, and chemisorption processes involved in the immobilization of organic compounds on mineral materials. It should also be mentioned that experiments on leaching sorbents to assess the potential for secondary water contamination by elements and compounds released from sorbents are often overlooked. To provide deeper insight into studying sorption mechanisms on sorptive mineral-organic components, we study sorbents like bentonite and lignite, which fundamentally differ in their sorption properties and interactions with sorbates. The main component of bentonite is montmorillonite. Isomorphous substitution of Si^{4+} by Al^{3+}/Fe^{3+} in tetrahedral sheets and Al^{3+} by Mg^{2+}, mainly in the octahedral sheets imparts a negative charge to the clay. This charge is compensated by cations in the interlayer spaces. The high cation exchange capacity of montmorillonite makes it an advantageous sorbent for cationic forms of non-organic and organic compounds, including drugs, dyes, and surfactants. With its ability to adsorb both anionic and cationic forms, lignite is a more versatile sorbet than bentonite. The use of both bentonite and lignite in a composite aims to create a hybrid sorbent, exploiting the sorption properties of both components. This approach could create versatile materials capable of removing various organic pollutants, including dyes, pharmaceuticals, and surfactants. To our knowledge, no studies have been conducted on such composite materials to remove dyes, pharmaceuticals, and surfactants from water and wastewater.

The primary goal of our work is to evaluate the removal efficiency of two dyes: Rhodamine b (RB) and Remazol brilliant blue r (RBBR); two pharmaceuticals: ibuprofen (IB) and sulfamethoxazole (STX); and the surfactant sodium dodecylbenzenesulfonate (SDBS) from water using a bentonite-lignite composite to deeply understand the influences of each component within the composite sorbent. We thoroughly investigated and described the sorption mechanisms using advanced instrumental analysis. Additionally, we characterized the sorbent's features to gain deeper insights into the interactions between the sorbent and sorbates. We also conducted a sorbent-leaching study to assess the potential of secondary water contamination from elements released from the sorbent. Lastly, we conducted sorption experiments with real wastewater to assess the effectiveness in removing RB, RBBR, IB, STX, and SDBS from the matrix solution. These results provide comprehensive insights into sorption behavior, interactions between sorbent and RB, RBBR, IB, STX, SDBS, and usability of bentonite-lignite composite in wastewater management scenarios.

2. Materials and methods

2.1. Materials

For each experiment, bentonite (BEN) from the Jelšovy Potok deposit in Slovakia, commercially available from Zębiec, Inc., with a size fraction of <0.2 mm and lignite (LIG) from the Bełchatów deposit in Poland, with a size fraction <0.4 mm, were used. Based on these materials, composites with varying sorbent contents were prepared by mechanically mixing the appropriate amounts of BEN and LIG in an agate mortar. We obtained and investigated the following homogeneous sorbent composites:

- BEN 80 wt % with LIG 20 wt % (BL 80:20)
- BEN 50 wt % with LIG 50 wt % (BL 50:50)
- BEN 20 wt % with LIG 80 wt % (BL 20:80).

Preliminary sorption experiments indicated that the BL 20:80 composite exhibited the best sorption affinity for the uptake of RB, RBBR, STX, and IB. Further explanations of these findings are provided in the "Sorption Results" section. Based on this conclusion, we focused our investigation solely on the BL 20:80 sample in subsequent sorption experiments and sorbent characterization presented in this study. Sorption studies were also conducted for BEN and LIG samples to understand the deeper implications of each component within the mineral composite.

2.2. Determination of physicochemical properties of sorbents

The cation exchange capacity (CEC) and anion exchange capacity (AEC) were determined. Procedures were performed in duplicate. For CEC determination, 1 g of sample was added to a 50 ml Falcon tube, followed by 45 ml of 1 M ammonium chloride (NH_4Cl). Mixtures were mechanically shaken for 3 h at 150 rpm and then left to undergo the cation exchange process for another 3 h. Samples were then centrifuged at 4500 rpm for 5 min, and the solutions decanted. Another 45 ml of 1 M NH_4Cl was then added to samples, stirred for 3 h, and left for an additional 3 h. The NH_4^+ sorption procedure was repeated three times. All samples were then washed twice with 20 ml of redistilled water and once with 20 ml of ethanol. Subsequently, the desorption procedure using 1 M sodium chloride (NaCl) was carried out. Materials were mixed with 45 ml of 1 M NaCl, shaken for 3 h, left for cation exchange for another 3 h, and centrifuged at 4500 rpm for 5 min. Solution from each Falcon tube was into a 200 ml volumetric flask for further NH_4^+ concentration analysis. The procedure described was repeated three times. For AEC determination, 800 mg of each sample was mixed with 40 ml of phosphate buffer containing 1 M of total PO_4^{3-} (as a source was KH_2PO_4 and K_2HPO_4) with pH 4.40 in Falcon tubes. The mixtures were shaken for 3 h and remained for anion exchange process conduction for the next 3 h. After that, samples were centrifuged at 4500 rpm for 5 min, and solutions were decanted. This process was repeated three times. Then, all sorbents were washed with 20 ml of redistilled water (twice) and 20 ml of ethanol (once). The next step was desorption using 1 M potassium nitrate (KNO_3) with pH 5.0. The materials were mixed with 45 ml of 1 M

KNO$_3$. Subsequently, mixtures were shaken for 3 h, remained for the next 3 h for anion exchange process conduction, and centrifuged at 4500 rpm for 5 min. The solution from each Falcon tube was decanted and collected in a 200 ml volumetric flask to analyze PO$_4^{3-}$ concentration further. This procedure was repeated three times. The CEC and AEC of the investigated sorbents were determined by calculating the amount of NH$_4^+$ and PO$_4^{3-}$ desorbed from the tested sorbents, respectively. NH$_4^+$ concentration was determined using Nessler's colorimetric method (Thompson and Morrison, 1951), while PO$_4^{3-}$ concentration was determined using the molybdenum blue colorimetric method (American Public Health Association, 1999) using a UV–Vis Hitachi U-1800 spectrophotometer.

The surface charge density was determined using potentiometric titration method as functions of solution pH and the point of zero charge (pH$_{ZPC}$). Examined suspensions were prepared with 1 g of the solid and 100 ml of electrolyte. Measurements were repeated three times for each selected system with three different electrolyte concentrations: 0.0001 M, 0.001 M, 0.01 M NaCl, with results averaged from these measurements for each sample. Systems were titrated with 0.1 M NaOH across a pH range of 3–10. This was performed using an Eco Titrator (Metrohm). The solid surface charge density (σ_0) was calculated using the following equation (Janusz, 1994):
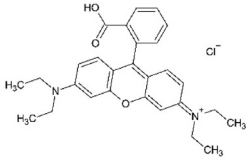
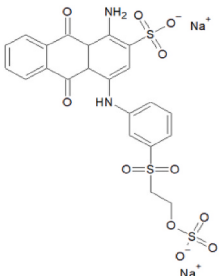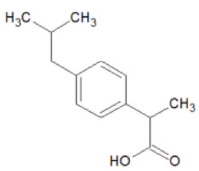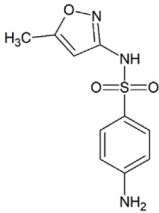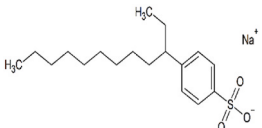$$\sigma_0 = (\Delta V \cdot c \cdot F)/(m \cdot S) \tag{1}$$

where ΔV is the volume difference of base added to achieve a specific pH in the suspension versus the supporting electrolyte solution [mL], c represents the concentration of the base [mol/L], F denotes the Faraday constant, m is the mass of the sorbent in the suspension [g], and S is the specific surface area of the solid [m^2/g].

Contact angle (CA) measurements were conducted using the sessile drop method with an automatic goniometer (Drop Shape Analyzer DSA25E). Redistilled water served as the reference liquid. Surface free energy (SFE) [mN/m] was determined through static CA measurements, using diiodomethane as another reference liquid. CA measurements were taken at room temperature following a stabilization period of 30 s. The mean CA for each liquid was calculated from five readings on each sample's surface. SFE calculations were based on Young's equation:

$$\gamma_S - \gamma_{SL} - \Pi_{eL} = \gamma_L \cos \theta_L \tag{2}$$

where γ_S is the solid-air SFE, γ_{SL} the solid-liquid interfacial energy, γ_L the liquid-air SFE, Π_{eL} the liquid film pressure, and θ_L the contact angle. The

Table 1
Characteristics of the organic compounds tested.

Compound	Structure	Molecular weight (ChemAxon, n.d.) [g/mol]	Molecular size (Pedretti et al., 2021) [Å]	Polar surface area (ChemAxon, n.d.) [Å^2]	pK$_a$ (ChemAxon, n.d.)	logK$_{ow}$ (ChemAxon, n.d.)
Rhodamine b (RB)		479.02	8.21x13.63x5.32	52.78	3.50 4.37	–
Remazol brilliant blue r (RBBR)		626.55	9.64x15.75x3.45	255.10	−0.41 14.91	–
Ibuprofen (IB)		206.27	4.32x10.29x3.10	37.3	4.86	3.84
Sulfamethoxazole (STX)		253.28	4.61x12.47x4.32	106.60	0.28 1.98 5.88	0.79
Sodium dodecylobenzenosulfonate (SDBS)		348.48	7.16x17.57x2.53	65.58	–	6.40

Abbreviations: pK$_a$ - exponent of acid dissociation constant; logK$_{ow}$ - octanol/water partition coefficient.

ADVANCE provided values for γ_{SL} and Π_{eL}.

2.3. Sorption experiments

In duplicate, batch sorption experiments for RB, RBBR, IB, STX, and SDBS were conducted at room temperature ($22 \pm 2^{\circ}$C). Characteristics of the sorbed compounds are presented in Table 1. After completing the sorption experiments, the equilibrium pH (pH$_{eq}$) of supernatants was measured. All sorption experiments used blank sorbate samples (sorbents with redistilled water without sorbates) as a reference. All reagents used were of analytical grade. Exceptions included high-purity acetonitrile and deionized water, which were essential for chromatographic analysis.

The initial experiments aimed to compare the sorption capabilities of composites BL 80:20, BL 50:50, and BL 20:80 for RB, RBBR, IB, and STX. These results selected the best composite (material with the highest RB, RBBR, IB, and STX adsorbed) with the appropriate BEN to LIG proportions for further investigation. In these experiments, 5 mL of RB and RBBR solutions, each with an initial concentration (C$_{in}$) of 500 mg/L, were mixed with 100 mg of each sorbent (20 g sorbent/L), whereas 5 mL of IB and STX solutions, each with a C$_{in}$ of 20 mg/L, were mixed with 50 mg of each sorbent (10 g sorbent/L). The initial pH of each solution was not adjusted and equaled 4.24 (RB), 7.01 (RBBR), 5.08 (STX), and 5.78 (IB). Because IB is poorly soluble in water (21 mg/L), (Yalkowsky and Dannenfleser, 1992) ethanol was mixed with redistilled water (1 v/v) to ensure that IB was completely dissolved. The initial pH's on the adsorption capacity of BEN, LIG, and BL 20:80 was investigated. BL 20:80 was identified as the most effective mineral composite for removing RB, RBBR, IB, and STX (based on sorption results interpretation of the experiment described above). The initial pH (pH$_{in}$) of all sorbate solutions was adjusted to range from 3 to 11. The pH$_{in}$ was adjusted using 0.1 M of hydrochloric acid (HCl) and 0.1 M of sodium hydroxide (NaOH). The 5 mL of RB and RBBR solutions (C$_{in}$ 500 mg/L) were mixed with 100 mg of each sorbent (20 g sorbent/L), and 5 mL of IB and STX solutions (C$_{in}$ 20 mg/L) were mixed with 50 mg of each sorbent (10 g sorbent/L). The effect of C$_{in}$ for RB, RBBR, IB, STX, and SDBS solution on BEN, LIG, and BL 20:80 adsorption capacity was also studied. The C$_{in}$ of IB and STX was 1–20 mg/L, the C$_{in}$ of RB and RBBR in the 10–500 mg/L range, and the C$_{in}$ of SDBS in the 5–100 mg/L range. 5 mL of RB, RBBR, and SDBS solutions were mixed with 100 mg of each sorbent (20 g sorbent/L) and 5 mL of IB, and STX solutions were combined with 50 mg of each sorbent (10 g sorbent/L). pH$_{in}$ of all sorbates was adjusted to 6. In all experiments described above, each sorbent material suspension with RB, RBBR, IB, STX, or SDBS was shaken for 24 h in a 7 mL plastic tube, centrifuged at 14000 rpm for 5 min, decanted, filtered (0.22 μm) and collected for the further quantified analysis.

Concentrations of RB and RBBR in filtered samples were determined using a UV–Vis Hitachi U-1800 spectrophotometer by spectrophotometric method. RB was measured at wavelength 554 nm, and RBBR at 594 nm. Concentrations of IB, STX, and SDBS in filtered samples were determined using reverse-phased high-performance liquid chromatography coupled with a diode array UV–Vis detector (HPLC-DAD/UV–Vis) Knauer K-2600 in isocratic elution mode. Details of the method are available in Table S1.

Sorption capacity S [mg/g] for the selected organic compound was calculated as follows:

$$S = \frac{(C_{in} - C_{eq})}{m} \bullet V \tag{3}$$

where C$_{in}$ is the initial concentration of each organic compound tested (considering blank sorbate samples) [mg/L], C$_{eq}$ the concentration of organic compound tested after adsorption [mg/L], V sorbate volume [L], and m sorbent mass [g].

2.4. Post-sorption material characterization

RB, RBBR, IB, STX, and SDBS sorption mechanisms were characterized for BL 20:80, BEN, and LIG samples after adsorption based on the nuclear magnetic resonance spectroscopy (NMR) results. An additional sorption experiment was conducted to obtain samples for NMR analysis. BL 20:80, BEN, and LIG were combined with 2 L sorbate solution containing RB, RBBR, IB, STX, and SDBS. Detailed sorption experimental conditions can be found in Table 2. Because this concentration of IB is not soluble in redistilled water, the IB solution was prepared by mixing water and ethanol in a 50:50 v/v ratio. Since STX is scarcely soluble in redistilled water at room temperature, the solution was prepared at 50°C. The suspensions were shaken for 24 h, mixtures were filtered through filter paper, and pH$_{eq}$ of the solutions was measured. Collected sorbents, as listed in Table 3, were dried at 30°C and homogenized, and then analyzed using NMR. ^{13}C CP MAS NMR spectra were recorded with a Bruker Avance III 500 MHz spectrometer (11.4 T). Samples were placed in 4 mm rotors and spun at 10 kHz. The samples were measured with cross-polarization at a resonance frequency of 125.8 MHz, 2 ms of contact time, 70–100% ramp amplitude, and SPINAL64 sequence for decoupling.

2.5. Sorbents leaching study

To evaluate the potential leaching of hazardous or environmentally risky metals and metalloids from the sorbents, 100 mg of BEN, LIG, and BL 20:80 samples were each mixed with 5 ml of redistilled water (pH 6) in a 7 mL plastic tube. The mixtures were shaken for 24 h. Subsequently, the suspension was centrifuged at 4700 rpm for 5 min, decanted, and filtered through a 0.22 μm filter. All tests were conducted in duplicate. Concentrations of various metals and metalloids [mg/L] in the filtered samples were determined using inductively coupled plasma optical emission spectrometry (ICP-OES) with a PerkinElmer Optima 7300 DV spectrometer.

2.6. Sorption experiments with wastewater from a municipal wastewater treatment plant

The effectiveness of the BL 20:80 composite as a sorbent was evaluated using treated wastewater from a municipal wastewater treatment plant in southern Poland (Table 4) mixed simultaneously with RB, RBBR, IB, STX, and SDBS. 30 mL of a stock multicomponent solution (pH$_{in}$ 8.01) containing wastewater with 50 mg/L of RB and RBBR, and 10 mg/L each of IB, STX, and SDBS, were mixed with 30 mg (1 g of sorbent/L), 150 mg (5 g of sorbent/L), and 300 mg (10 g of sorbent/L) of BL 20:80, respectively, in 50 mL plastic tubes. Mixtures were prepared in triplicate and shaken for 24 h at room temperature (22 ± 2 °C). Subsequently, supernatants were centrifuged at 4500 rpm for 5 min, decanted, filtered through a 0.22 μm filter, and collected for further quantified and pH$_{eq}$ analysis. A blank stock solution was used as a reference. Concentrations of RB, RBBR, IB, STX, and SDBS in filtered samples were determined using liquid chromatography coupled with triple quadrupole mass spectrometry (LC-MS/MS) with an Agilent Tech. 1290 Infiniti, 6460 TripleQuad system. Multiple reaction monitoring was employed. Three analytical methods were developed to simultaneously analyze RB with STX, RBBR with SDBS, and IB separately. Details of the method are available in Table S2.

2.7. Analytical methods

X-ray diffraction (XRD) powder patterns were obtained using a Rigaku SmartLab diffractometer with graphite-monochromatized CuKα radiation. For qualitative phase analysis, settings were adjusted to 0.05°2θ step with a 1 s/step counting time. For quantitative analysis, settings were set to a 0.02°2θ step with a 2 s/step counting time. For quantitative X-ray analyses, 10 wt% ZnO was added to the samples as an

Table 2
Detailed conditions of sorption experiments (Solińska et al., 2023).

	RB	RBBR	IB	STX	SDBS
Initial concentration [mg/L]	2000	1000	500	500	1500
Initial pH	3.00	5.50	4.44	4.39	7.08
Solvent for sorbate solution	redistilled water	redistilled water	redistilled water and ethanol (50:50 v/v)	redistilled water at 50°C	redistilled water
Sorbent amount per 2 L of sorbate [mg]	400	400	200	200	300

Table 3
The symbols of sorbent samples with adsorbed organic compounds.

sorbate / sorbent	BEN	LIG	BL 20:80
RB	BEN-RB	LIG-RB	BL 20:80-RB
RBBR	BEN-RBBR	LIG-RBBR	BL 20:80-RBBR
IB	BEN-IB	LIG-IB	BL 20:80-IB
STX	BEN-STX	LIG-STX	BL 20:80-STX
SDBS	BEN-SDBS	LIG-SDBS	BL 20:80-SDBS

internal standard, and the mixture was homogenized using a McCrone mill. "Side loading" samples were prepared from such a material to ensure the best crystallite disorientation. Analysis was conducted using the standardless Rietveld method with SiroQuant software. Quantitative chemical composition was determined using ZSX Primus II Rigaku spectrometer for wavelength dispersive X-ray fluorescence (XRF) with a rhodium (Rh) anode as an X-ray source. TOC concentration was calculated by subtracting inorganic carbon (IC) content from total carbon (TC) content. TC and IC content of tested samples were measured using a TOC - V CPH total organic carbon analyzer connected with Solid Sample Module SSM-5000A. Thermal analysis (differential thermal analysis [DTA]/thermogravimetry [TG]) coupled with evolved gas composition determination was conducted on a Netzsch STA 449 F3 Jupiter apparatus. Analysis was conducted at the rate of 10 K/min under a dynamic helium (He) atmosphere flow (50 ml/min) at 25–1000 °C. The composition of gases evolved during sample decomposition was analyzed by a 403C Aeolos QMS quadrupole mass spectrometer and an FTIR Bruker Tensor 27 spectrometer. The mass spectrometry analysis was carried out in the scan mode for m/z (where m is the molecule's mass and z is the molecule's charge in electron charge units) in the range of 10–100. Morphology of gold-coated samples was observed using a FEI 200 Quanta field emission scanning electron microscope.

2.8. Determination of the textural parameters

Textural parameters were determined using low-temperature N_2 adsorption/desorption isotherms at -196°C with an Accelerated Surface Area and Porosity (ASAP) analyzer by Micromeritics. Before measurements, samples were outgassed for 24 h at 100°C. Based on the data collected from N_2 isotherms, specific surface area (S_{BET}) was calculated using the Brunauer–Emmett–Teller (BET) equation (Brunauer et al., 1938). Total pore volume ($V_{tot}^{0.99}$) was calculated from the N_2 adsorbed at a relative vapor pressure (P/P_0) of about 0.99. Micropores volume (V_{mic}^{DR}) was determined using the Dubinin–Radushkevich method (Dubinin, 1960). Mesopore volume (V_{mes}^{BJH}) was calculated using the BJH (Barrett–Joyner–Halenda) method (Barrett et al., 1951) from the adsorption branch in the range designated for mesopores according to Dubinin (1960). Macropore volume (V_{mac}) was calculated using the equation:

$$V_{mac} = V_{tot}^{0.99} - (V_{mic}^{DR} + V_{mes}^{BJH}) \tag{4}$$

The BJH (Barrett–Joyner–Halenda) method evaluated the pore size distributions based on the isotherms' adsorption branch (Barrett et al., 1951).

3. Results and discussion

3.1. Characterization of sorbents

The chemical composition of LIG and BEN, the source materials for the BL 20:80 composite, are presented in Table 5. The predominant chemical components in BEN are Si and Al, which form $[SiO_4]$ tetrahedral and $[AlO_3]$ octahedral units in a smectite structure. The significant concentration of Fe_2O_3 ($\sim$12 wt%) may be due to the substitution of Si^{4+} by Fe^{3+} in tetrahedral layers and Al^{3+} by Fe^{3+}/Fe^{2+} in octahedral layers. This leads to a negatively charged surface on smectites. The exhibited amounts of Ca, Na, and K form cations that compensate for the negative charge of this clay mineral and contribute to the cation exchange sorption mechanism. In LIG, the loss of ignition (LOI $\sim$80 wt%) indicates a high content of organic compounds. The remaining elements consist of admixtures incorporated into organic materials and mineral phases like kaolinite, gypsum, quartz, and Fe-based minerals (refer to the XRD results).

The concentration of IC and TOC in the sorbents are shown in Table 6. The LIG sample contains approximately 43 wt% TOC. This confirms a significant presence of organic matter within the lignite structure. The negligible amount of IC indicates the presence of mineral phases containing carbon. For BEN, the IC content (0.46 wt%) is higher than TOC (0.01 wt%), yet it is still considered negligible. The IC value suggests the presence of some mineral phases containing carbon in the BEN sample.

Quantitative analyses of BEN and LIG samples, revealing their phase compositions, were conducted using XRD results. The main phase in BEN (58 wt%) was the clay mineral montmorillonite, from the smectite group (Fig. 1). Montmorillonite is well-known and documented as the dominant clay mineral in the Jelšovy Potok deposit (Breen et al., 1995; Madejová et al., 1996; Tkac et al., 1994). The XRD pattern for the air-dried sample showed that the [001] diffraction peak at 15.3 Å may indicate Ca^{2+} primarily occurring in the interlayer spaces of montmorillonite. BEN also contained 25 wt% amorphous phase, along admixtures of illite (10 wt%), quartz (4 wt%), calcite (3 wt%), and plagioclases (<1 wt%). In LIG, the amorphous phase dominates (91 wt%), associated with a significant presence of organic matters in lignite. Typically, these organic substances lack crystalline, well-ordered structures. The LIG sample contained admixtures of kaolinite (6 wt%), gypsum (2 wt%), quartz (1 wt%), and Fe-based minerals: hematite, goethite, and pyrite (each <1 wt%). The XRD pattern of BL 20:80 showed relatively fewer mineral phases peaks compared to BEN and LIG. This visible pertains to phases from the BEN sample. This lower presence of mineral phases in the composite results from mixing 20 wt% BEN with 80 wt% LIG.

Table 4
The main chemical data of the wastewater from municipal wastewater treatment plant.

	SO_4^{2-} [mg/L]	Fe [mg/L]	Zn [mg/L]	NO_3^- [mg/L]	NH_4^+ [mg/L]	Cl^- [mg/L]	PO_4^{3-} [mg/L]	TOC [mg/L]	COD [mgO$_2$/L]	BOD [mg O$_2$/L]
Concentration	100	3.21	0.26	0.68	47.84	138	8.29	34.1	33.1	5.8

Abbreviations: TOC – total organic carbon, COD – chemical oxygen demand, BOD – biological oxygen demand.

Table 5
Chemical composition of LIG and BEN sample.

Sample	SiO$_2$	TiO$_2$	Al$_2$O$_3$	Fe$_2$O$_3$	CaO	MgO	MnO [wt.%]	Na$_2$O	K$_2$O	P$_2$O$_5$	SO$_3$	ZnO	LOI
LIG	5.43	0.08	4.75	1.23	4.50	0.18	0.01	b.d.	0.02	0.03	3.75	0.09	79.84
BEN	36.69	1.47	32.56	12.03	1.30	0.20	0.21	0.09	0.17	0.53	0.13	0.02	9.53

Abbreviations: b.d. – below detection limit.

Table 6
TC, IC, and TOC of LIG and BEN samples.

Sample	TC [%]	IC [%]	TOC [%]
BEN	0.47	0.46	0.01
LIG	43.3	0.01	43.3

The FTIR spectra of evolved gases at different temperatures for BEN, LIG, and BL 20:80 are shown in Fig. 2. CO_2 and H_2O are the two major gaseous compounds released from BEN, LIG, and BL 20:80 samples during heating. They originate from the decomposition of organic compounds adsorbed on the sorbents or carbon in LIG and water within the structure of their constituent minerals (clay minerals, goethite, gypsum). Characteristic water bands in FTIR spectra are observed in the broad ranges of 4020–3400 cm^{-1} and 2070–1250 cm^{-1}, along with characteristic CO_2 peaks (2366, 2338–2332, and 670 cm^{-1}) indicate that below 200 °C, only water and carbon dioxide were evolved from the BEN, LIG, and BL 20:80 samples. Characteristic peaks for CO (2190–2183 and 2105–2096 cm^{-1}) appeared at 280–300 °C and had maximum absorbance at 750 °C. Bands from CO appear only in the LIG and BL 20:80 spectra, indicating their organic origin related to LIG material. This agrees with the TOC content in LIG, which is 43.3%, compared to only 0.01% in BEN (Table 6). Bands at 3080, 3012, and 2935 cm^{-1} in LIG and BL 20:80 samples, caused by C–H, C=C-H, and -CH$_3$ stretching vibrations, respectively, occur widely in organic material, indicating the onset of formation and emission of various organic compounds at 300–330 °C with maximum absorbance at 480–500 °C. Bands originating from C-H bonds vibrations are mainly related to organic matter in the LIG sample.

The SEM images of BEN reveal montmorillonite minerals forming plate-like grains smaller than 5 μm (Fig. 3a). These plates are tightly packed, forming aggregates resembling paper or tissue. The LIG images, the irregular, oval-like, and elongated particles with up to 800 μm in size are observed (Fig. 3b). The images also show transformed parts of raw phytomass and organic matter, comprising the LIG sample. In BL 20:80, montmorillonite grains form compacted aggregates on the surface of LIG particles (Fig. 3c). A noticeable difference in grain size between BEN and LIG sorbents is also observed.

The N$_2$ adsorption/desorption isotherms for BEN and BL 20:80 (Fig. 4) are type IV with H3 hysteresis loop, according to IUPAC classification (Sing et al., 1995). Such textural features are characteristic for mesoporous materials with slit-like pores. This characterizes of bentonite, the dominant component in the BEN sample. The main component of bentonite is smectite group minerals with a characteristic texture resembling a tissue layer. The isotherm shape for the LIG sorbent is a type II with an H4 hysteresis loop, attributed to materials with negligible porosity and narrow slit-like pores. For BEN, three pore sizes were identified. The initial shape of the N$_2$ isotherm at low P/P$_0$ (0 up to ~0.2) suggests micropores. The existing hysteresis loop and increased N$_2$ adsorption at high P/P$_0$ confirm mesopores (P/P$_0$ 0.4–0.95) and macropores (P/P$_0$ above 0.95). The observations align with the BEN sample's pore size distribution curve, reflecting changes in pore diameter (Fig. S1). BEN's S$_{BET}$ was 47.6 m^2/g, with micropore volume at 0.059 cm^3/g, mesopores at 0.019 cm^3/g, and macropores at 0.026 cm^3/g (Table 7). The shape of the N$_2$ isotherm and pore size distribution curve of LIG indicates the occurrence of only mesopores and macropores. LIG exhibited negligible porosity with an S$_{BET}$ of only 3.2 m^2/g and a V$_{tot}^{0.99}$ of 0.019 cm^3/g. The volume of mesopores (0.010 cm^3/g)
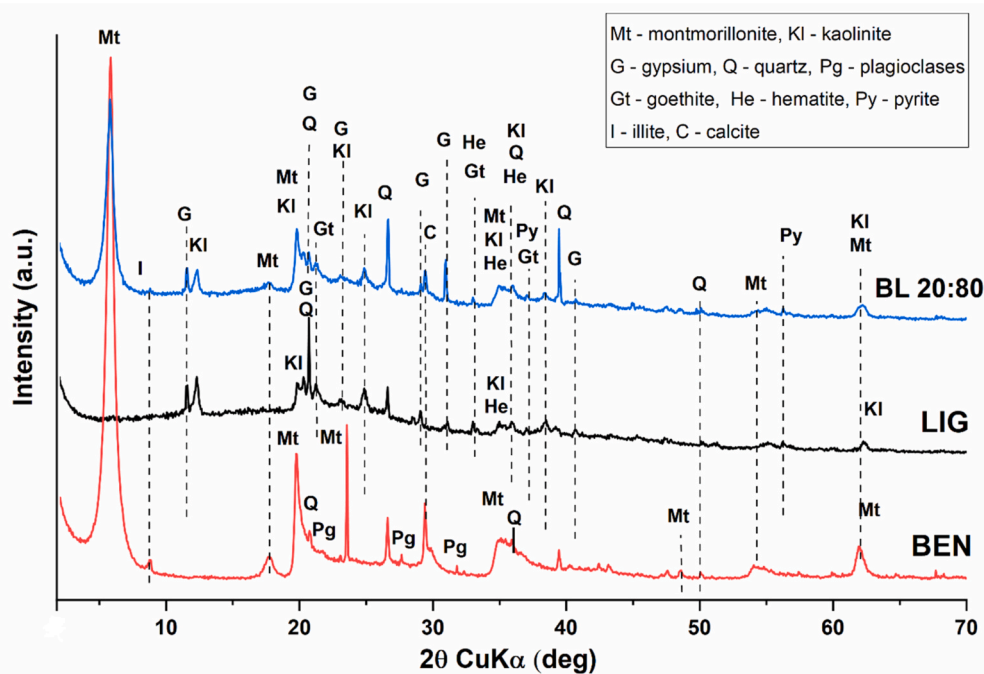
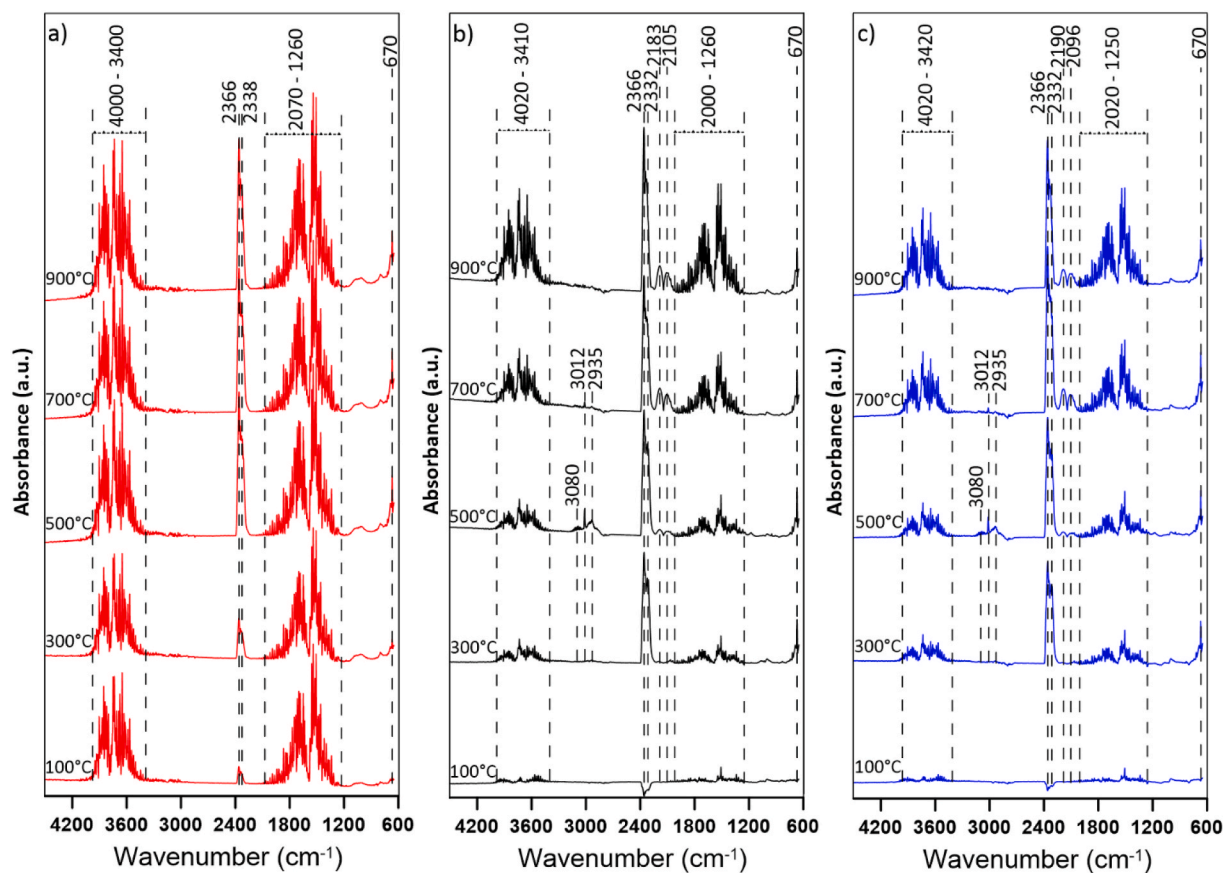

Fig. 1. XRD patterns of BEN, LIG, and BL 20:80.

Fig. 2. FTIR spectra of the gaseous species of the evolved gases at different temperatures in He for a) BEN, b) LIG, c) BL 20:80.

prevailed. Such low porosity and S_{BET} values were previously reported for lignite from the Bełchatów deposit (Henc et al., 2018). BL 20:80 properties average the textural parameter of the sorbents described above. The higher LIG content compared to BEN in the composite resulted in relatively small porosity. The S_{BET} of BL 20:80 was 11.8 m^2/g, with $V_{tot}^{0.99}$ of 11.8 cm^3/g, lower than BEN's but higher than LIG's. In the composite amount of micropores and mesopores was smaller than BEN. Conversely, the mesopores amount was slightly increased (Table 7). This may be influenced by the specific arrangement of grains from both sorbents in the composite.

3.2. Physicochemical properties of sorbents

The AEC of LIG is 7.54 meq/100g, while BEN's only 0.66 meq/100g (Table 8). This indicates that LIG has significant anion-exchanging abilities, whereas BEN has minimal. The CEC of BEN and LIG is similar, 74.21 and LIG 83.01 meq/100g, respectively, and relatively high. The organic structure of lignite materials is unique, heterogeneous, and complex, so it causes different phenomena responsible for their ionic exchangeable properties to occur. Low-rank coal, such as LIG, consists of aromatic-based copolymer molecules with cross-linked covalent and non-covalent bonds. These molecules contain oxygen, sulfur, nitrogen heteroatoms, and numerous functional groups linked to aromatic and cyclic rings (Vasireddy et al., 2011). Active groups with varying polarities, such as carboxylic, phenolic, ether, ester, carbonyl, and hydroxylic groups, can facilitate cation exchange. Specifically, the acidic nature of hydroxyl (-OH) and carboxyl (-COOH) groups facilitates cation removal through ion exchange by replacing hydrogen proton. The protonation of amine groups and the natural presence of NH_3^+ groups in lignite material impart anion exchange properties to LIG. The admixture of Fe-based minerals in LIG might also contribute to anion exchange

properties. Like other clay minerals, BEN is characterized by a permanently negative surface charge, balanced by exchangeable cations. In the case of BEN, this could be Ca^{2+}, as indicated by our studies. This means it has a weak affinity for anions removal. However, it exhibits a high affinity for cation removal. Consequently, the AEC of BL 20:80 is lower than that of LIG. Despite the high CEC values for BEN and LIG, a decrease in CEC was observed for BL at 20:80. It might be related to interactions between BEN and LIG in composite blocking access to cation exchangeable sites.

Potentiometric titration results indicate that the pH_{ZPC} values for BEN, LIG, and BL 20:80 are approximately 4.4, 3.2, and 3.3, respectively. This indicates that at these pH values, the surfaces of the sorbents exhibit zero net surface charge (Fig. S2). The quantities of positive and negative surface groups are nearly identical. At pH values below pH_{ZPC}, the solid surfaces become positively charged; conversely, at pH values above the pH_{ZPC}, they become negatively charged. LIG exhibits the highest negative charge density, while BEN shows the lowest. The pH_{ZPC} value for BEN is slightly higher than those reported in the literature (pH_{ZPC} 2–4), though much higher values (7.6–8.1) have also been reported (Rozalén et al., 2009). The pH_{ZPC} value for LIG aligns with those documented in the literature (Wang et al., 2017). For the BL 20:80 composite, the pH_{ZPC} value is influenced by the presence of LIG.

To assess the hydrophobicity/hydrophilicity property of tested sorbents, CA was decreased from 58.9° for LIG to 45.5° for BL 20:80 and to 20.5° for BEN. A higher CA indicates greater hydrophobicity of the sorbent surface. Based on these results, BEN appears to be a favorable sorbent for adsorbing polar organic compounds, while LIG is suited for nonpolar organic compounds. BL 20:80 is expected to adsorb both polar and nonpolar forms of organic compounds. An increase in CA can lead to a reduction in the SFE sorbents. This is consistent with SFE values for LIG, BL 20:80, and BEN, which are 51.2, 59.3, and 72.9 mN/m,
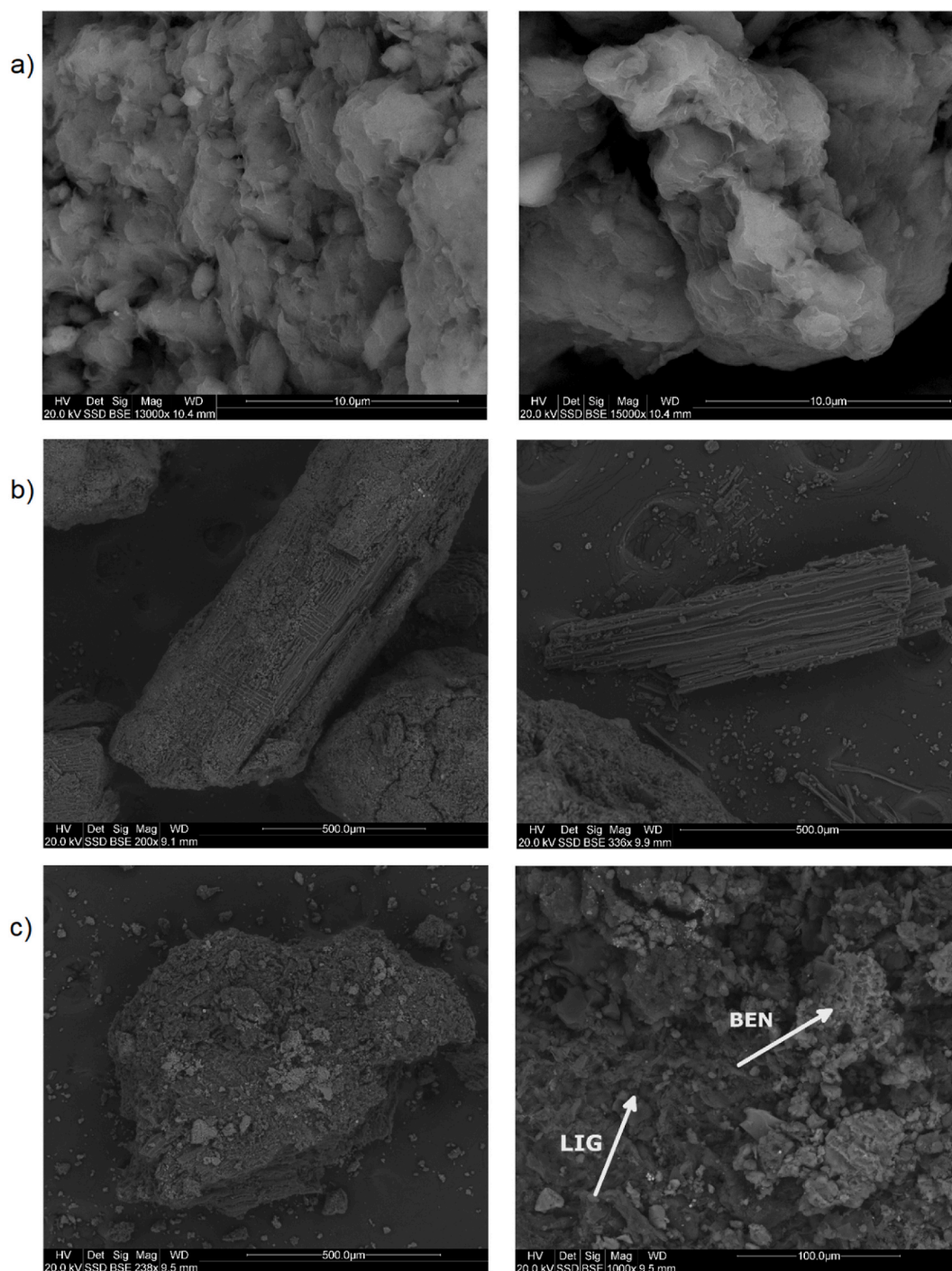
Fig. 3. SEM images for: a) BEN, b) LIG, c) BL 20:80.

respectively. SFE is the driving force behind the adsorption of water and generally polar compounds.

3.3. Sorption results

The outcomes of the initial sorption experiments enabled verification of the optimal BEN to LIG ratio for creating the best mineral composite for subsequent sorption experiments. The sorption results for dyes indicate that increasing BEN's proportion in composites negatively affects RBBR sorption (Fig. 5). Under the set sorption conditions, RBBR existed as an anion and might have encountered limited anionic sorption capacity in BEN, given its negligible AEC (Table 8). The BL 20:80

mixture adsorbed RBBR at 7.5 mg/g (33% efficiency), while BL 80:20 achieved 4 mg/g (17% efficiency). Conversely, RB adsorption was consistent at 22 mg/g (99% efficiency) across all composite sorbents. The cationic charge on RB's N^+ could contribute to its strong cationic exchange affinity towards LIG and BEN, both characterized by high CEC values (Table 8). Notably, sorption results were better for RB than for RBBR.

For pharmaceuticals, the adsorption of IB and STX decreased with an increased proportion of BEN in the composites. Notably, the BL 80:20 composite does not adsorb IB at all. The hydrophilic properties of BEN (see Chapter 3.2) lead to the repulsion of IB, which is relatively hydrophobic, as indicated by its $logK_{ow}$ value of 3.84. Additionally, BL 20:80
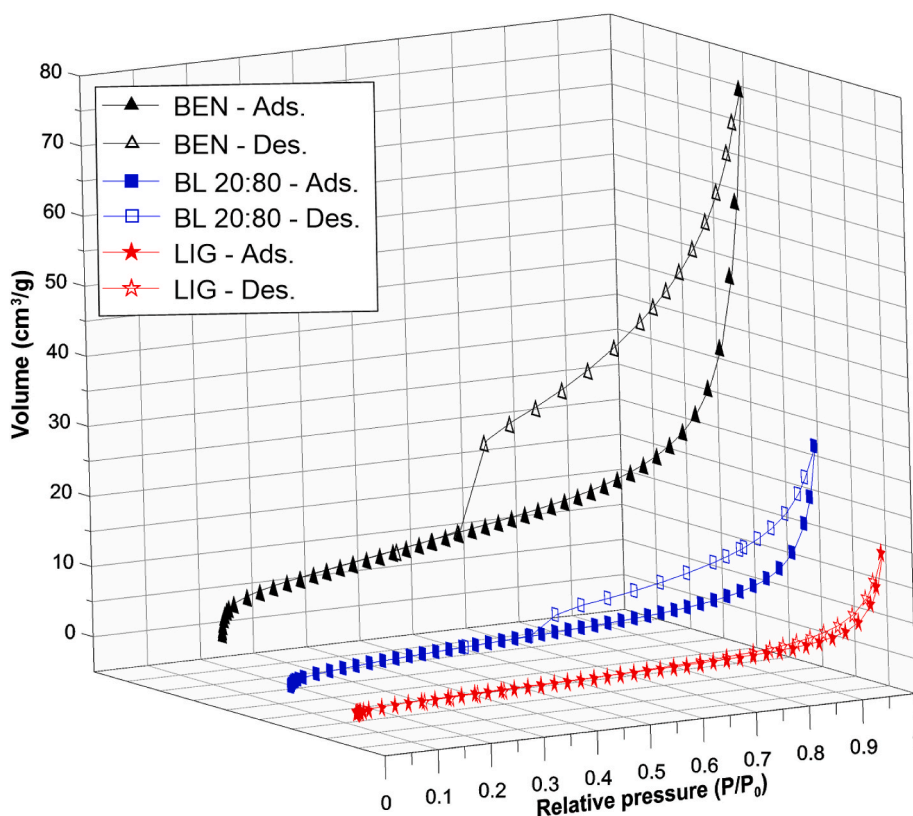
Fig. 4. N$_2$ adsorption isotherms for BEN, LIG, and BL 20:80.

Table 7
Textural parameters for BEN, LIG, and BL 20:80.

	S$_{BET}$ [m^2/g]	V$_{tot}^{0.99}$ [cm^3/g]	V$_{mic}^{DR}$ [cm^3/g]	V$_{mes}^{BJH}$ [cm^3/g]	V$_{mac}$ [cm^3/g]
LIG	3.2	0.019	0.001	0.010	0.008
BEN	47.6	0.104	0.059	0.019	0.026
BL 20:80	11.8	0.036	0.004	0.020	0.012

Table 8
Values of CEC and AEC for BEN, LIG, and BL 20:80 samples.

Sample	LIG	BEN	BL 20:80
AEC [meq/100g]	7.54	0.66	4.28
CEC [meq/100g]	83.01	74.21	65.12

removed more IB than STX. In this composite, 1.75 mg/g of IB (72% efficiency) and 1.40 mg/g of STX (75% efficiency) were adsorbed. The results indicate that BL 20:80 is the most effective mineral sorbent composite. This composite was utilized in subsequent experiments, the results of which are detailed in the next section of this paper.

The sorption of RBBR on LIG remains constant at 8–9 mg/g for pH$_{in}$ 3-9, with an increase to 20 mg/g at pH$_{in}$ 11 (Fig. 6). The pH$_{eq}$ of 3.9–4.0 indicates LIG's ability to buffer pH changes. However, it is expected reaction's behavior is initially controlled by the pH$_{in}$ of each solution. Sorption on BL 20:80 occurs at a similar level and varies similarly with pH, exhibiting an equilibrium pH of 4.4–4.5. For BEN, the highest sorption of RBBR occurs at pH$_{in}$ 5-9 (12–16 mg/g), while at the extremes of pH$_{in}$ 3 and 11, sorption is 5 and 4 mg/g, respectively. At pH 4–5, following the reaction of RBBR with LIG and BL 20:80, a strong electrostatic interaction occurs between the protonated binding sites of the adsorbent and the negatively charged dye molecules (Fig. 7). This phenomenon does not explain the significant sorption observed for BEN at pH$_{in}$ 5-9 with a basic pH$_{eq}$. Considering BEN's higher pH$_{ZPC}$ (4.4)

compared to LIG (3.2) and BL 20:80 (3.3), more protonated sites are available for the anion form of RBBR molecules in the initial minutes of the sorption reaction. This suggests that the initial conditions of the reaction primarily influence the sorption of this dye. As the pH$_{in}$ increases to 11, adsorbent surface active sites become deprotonated due an excess of OH$^-$ ions. This increases the number of negatively charged sites on the adsorbent surface, potentially leading to increased electrostatic repulsion between RBBR and the permanently negatively charged BEN surface. Furthermore, the reduced sorption of RBBR with increasing pH stems from competition between hydroxyl ions and anion dye ions for adsorption sites (Debamita et al., 2020). For LIG and BL 20:80, the high RBBR adsorption at pH$_{in}$ = 11 may be attributed to hydrogen bonding between RBBR's amine and sulfonic and LIG, as well as dispersion and π-π interaction between their aromatic rings (Solińska et al., 2023).

Sorption of RB on LIG remains consistent within the pH$_{in}$ range of 3–11, resulting in an pH$_{eq}$ 3.8–4.1 (Fig. 6). BL 20:80 and BEN showed higher sorption with pH$_{eq}$ values of 4.5–4.6 and 8.0–9.7, respectively. Given that the structure of RB changes with pHs (Fig. 7), its adsorption behavior is complex. At pH > 4, observed across all studied sorbent-RB systems, the dye exists in a protonated/deprotonated state, as a zwitterion (RB±) (Shakir et al., 2010), with the positive and negative charges located at the =N$^+$ and COO$^-$, respectively. A specific electrostatic attraction occurs between the negatively charged adsorbent surfaces and the positive sites at the =N$^+$ (Eftekhari et al., 2010). Under the
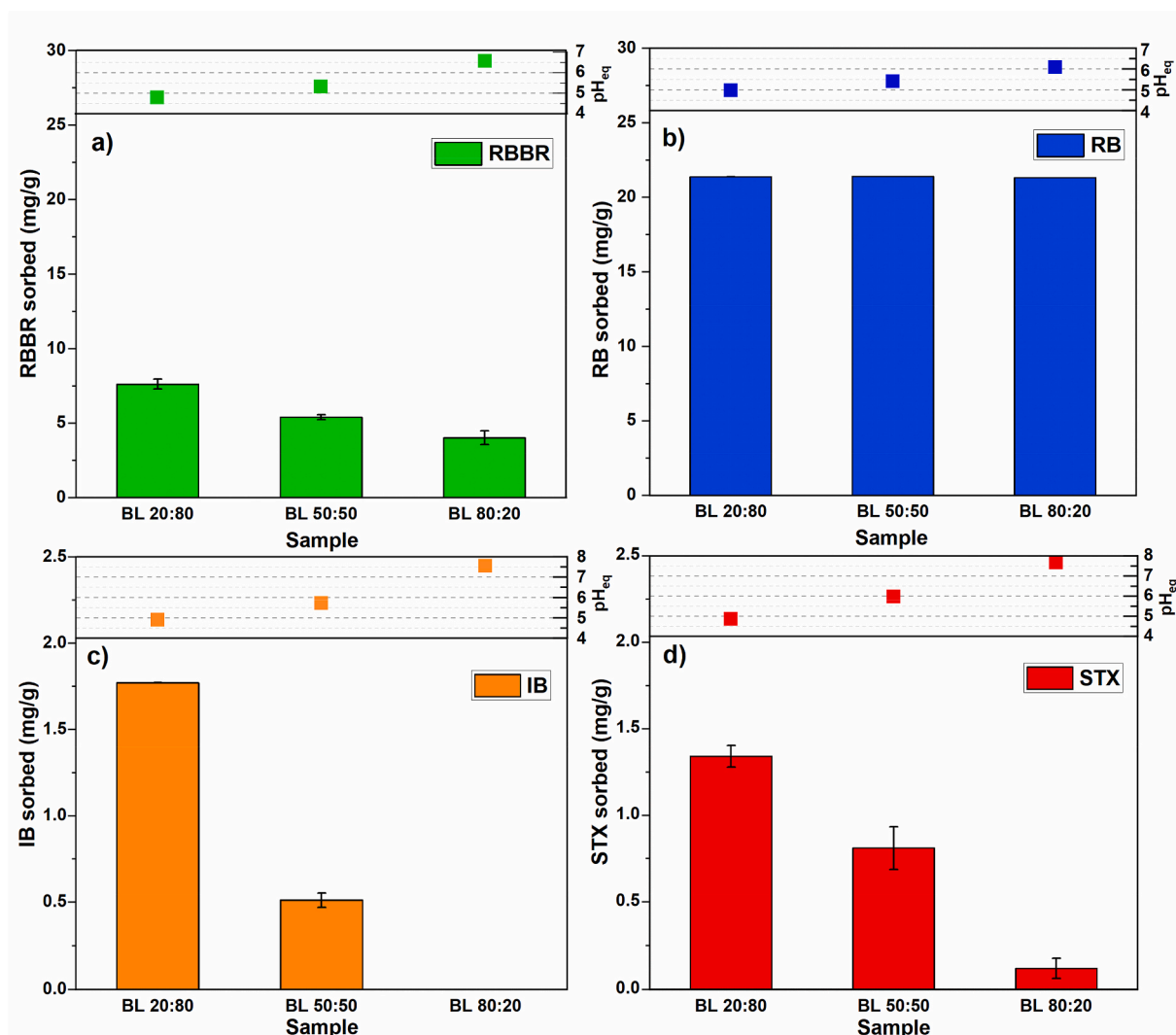
Fig. 5. The a) RBBR, b) RB, c) IB, and d) STX sorption results on mineral composite as the function of different proportions of BEN to LIG. The values above the sorption graphs indicate pH_{eq}.

experimental conditions (pH > 4) the negative surface charge of the sorbents is influenced by their pH_{ZPC} values: 4.4 for BEN, 3.2 for LIG, and 3.3 for BL 20:80. BEN possessing the largest specific surface area (Table 7), offers more active sites for adsorption, contributing to its higher RB sorption capacity (Fig. 6).

The sorption of IB on LIG remains generally across pH_{in} 3-9. However, it's notable that the pH_{eq} is 4.0–4.2, reflecting LIG's pH buffering effect. A slight increase of IB adsorption is observed at pH_{in} 11 (Fig. 6). Sorption of IB on BL 20:80 increases as pH_{in} rises from 3 to 11, and the pH_{eq} is also within a narrow range of 4.4–4.7. For BEN, IB is adsorbed in small amounts across the entire pH_{in} range with an pH_{eq} ranging from 8.2 to 10.5. In general, the amount of IB sorption slightly increases with increasing pH_{in}, regardless of the type of sorbent (Fig. 6). IB with pKa of 4.86, suggests most of its molecules are neutrally charged at pH < 4.86, as presented in Fig. 7. Therefore, it can be inferred that the negatively charged LIG (pH_{ZPC} 3.2) and BL 20:80 (pH_{ZPC} 3.3) may not facilitate high-efficiency sorption of IB below pH 4.96. The main mechanism responsible for IB removal is attributed to physical sorption. As CA values of LIG (58.9°) and BL 20:80 (45.5°), and the value of log K_{ow} for IB (3.84) suggest their hydrophobic properties may involve hydrophobic interaction IB-LIG and IB-BL 20:80. The carboxyl group in IB's structure facilitates electrostatic forces and hydrogen bonding during in its adsorption on LIG and BL 20:80. π-π interactions may occur between IB and the aromatic rings of LIG and BL 20:80 sorbents. In alkaline

conditions, the dissociation degree of the surface groups of the BEN (pH_{eq} is 8.2–10.5) and IB is high, leading to mutual repulsion due to both being negatively charged.

The sorption of STX on LIG and BL 20:80 remains constant at 1.3–1.5 mg/g across the entire pH range, with pH_{eq} values of 4.0–4.2 and 4.3–4.6, respectively. Sorption of STX on BEN is negligible across the entire pH_{in} range, varying from 8.3 to 10.6 in the equilibrium solution. STX predominantly exists as a cation (Fig. 7) at pH below 1.98; between pH 1.98 and 5.88, the molecule is characterized by a neutral charge, and above pH 5.88, becomes negatively charged (Avisar et al., 2010). At pH > 3.2–3.3 LIG and BL 20:80 are negatively charged, so at pH_{eq} 4.0–4.6, the negatively charged sorbent surface interact with neutrally charged STX molecules. The physical sorption process likely plays a key role in STX immobilization on LIG and BL 20:80. STX, containing a sulfonamide unit and isoxazole ring, interacts via hydrogen bonding and electrostatic forces with N, O heteroatoms, and ester, ether, and carboxylic groups in LIG's structure. Conversely, a negatively charged surface of BEN interacts with negatively charged STX molecules, leading to mutual repulsion. These results align with studies showing sulfonamide compounds, including STX, are weakly absorbed by mineral soil colloids (Thiele-Bruhn et al., 2004).

The maximum sorption of RBBR on LIG, BEN, and BL 20:80, within the initial concentration range of 10–500 mg/L, reaches similar levels of 8.5, 6.9, and 7.2 mg/g, respectively (Fig. 8). However, adsorption of
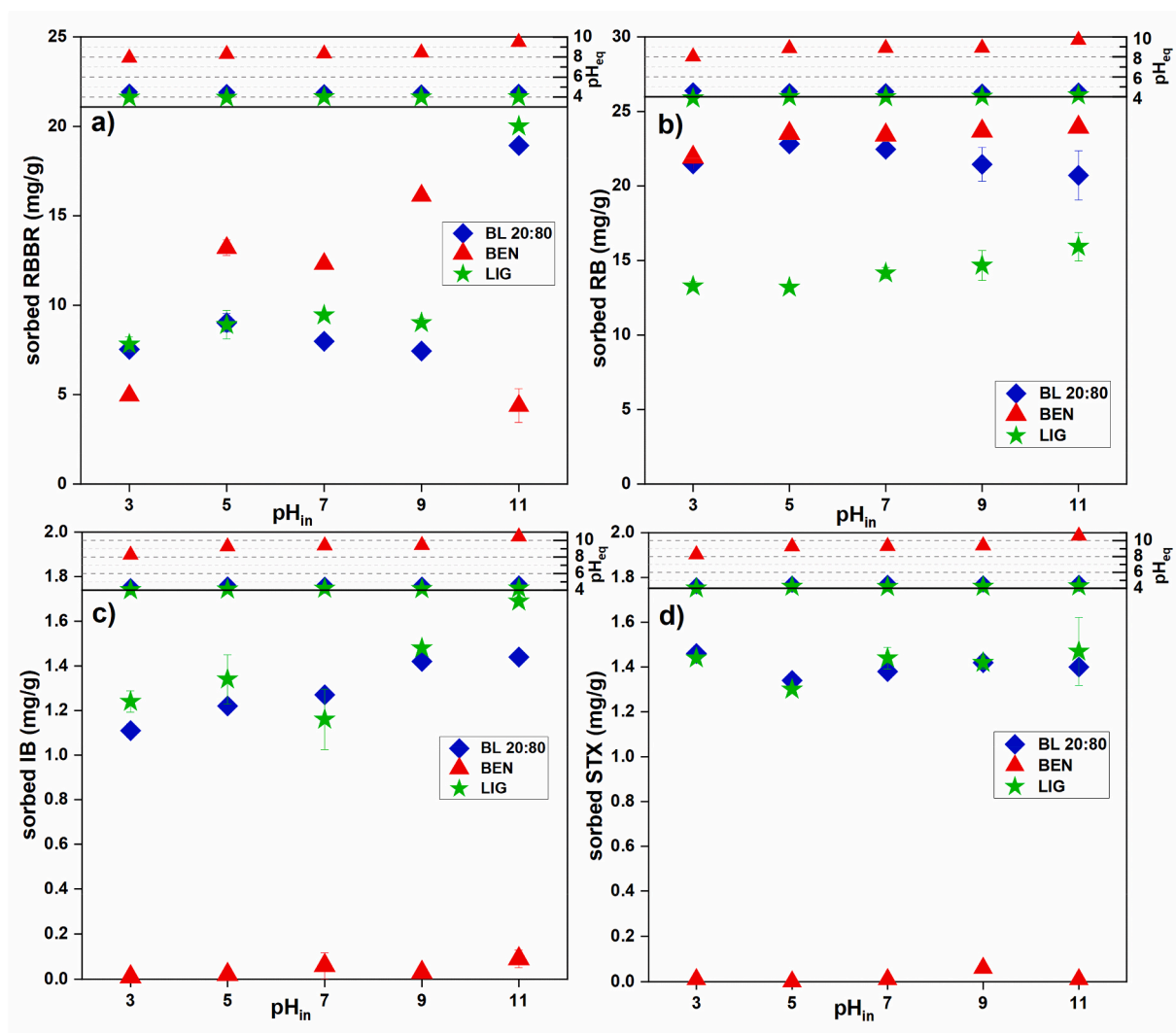
Fig. 6. The a) RBBR, b) RB, c) IB, and d) STX sorption results on BEN, LIG, and BL 20:80 as the function of different pH_{in} of sorbates. The values above the sorption graphs indicate pH_{eq}.

RBBR increases with higher C_{in}, regardless of the sorbents. pH_{eq} after sorption is 4.8 for LIG and 4.6 for BL 20:80, while for BEN, it becomes alkaline (above 8). Given the pH_{ZPC} values of the sorbents range from 3.2 to 4.4, at the observed pH_{eq} their surfaces acquire a negative charge. This leads to electrostatic repulsion between negatively charged RBBR (Fig. 7) and the sorbent surface, limiting higher dye adsorption. Nevertheless, the higher AEC of LIG and BL 20:80, compared to BEN (Table 8), contributes to a slightly higher adsorption of anionic RBBR, as indicated by the results. Sorption of LIG involves hydrogen bonding between RBBR's sulfonic/amine groups and LIG, as well as dispersion and π-π interaction between RBBR's aromatic rings and LIG, contributing to RBBR uptake. These mechanisms similarly apply to sorption on BL 20:80, given the predominance of LIG content in the composite.

BEN and BL 20:80 are significantly more effective RB sorbents than LIG. BEN and BL 20:80 adsorbed up to 22.3 mg RB/g, achieving over 99% efficiency, compared to LIG's 15 mg/g (70% efficiency). Above pH 4, RB predominantly exists as a zwitterion (RB±) in solution. With post-reaction pH_{eq} values of 9.2 for BEN and 4.7 for BL 20:80. This predisposes BL 20:80 to higher sorption efficiency, as its pH_{eq} of 4.7 is near the pH 3 limit where RB begins to show as positively charged (RBH⁺) (Shakir et al., 2010). The dependence of surface charge on solution pH (Fig. S2), BEN possesses a less negative charge than BL 20:80 but has a higher specific surface area. This results in a greater surface charge on BEN, capable of electrostatic interaction with RB. The lower sorption

capacity of LIG is primarily attributed to its small S_{BET} of 3.2 m²/g.

LIG and BL 20:80 are more effective IB sorbents, each retaining the pharmaceutical at 1.5 mg/g, in contrast to the significantly lower sorption on BEN at 0.2 mg/g. Maximum sorption capacity was not reached for either LIG or BL 20:80. The pH_{eq} after reaction is 4.8 for LIG and 4.5 for BL 20:80, indicating both materials are relatively suitable as IB sorbents, with negative charges starting at pH_{ZPC} values of 3.2 for LIG and 3.3 for BL 20:80. The hydrophobic characteristics of LIG and BL 20:80 can promote interaction with IB's low polarity moieties (logK$_{ow}$ 3.84). The presence of methyl group and aromatic rings in IB's structure suggests that dispersion forces also play a role in its sorption onto LIG and BL 20:80. With a pH_{eq} of 9.4, BEN acquires a negative charge (pH_{ZPC} 4.4), leading to mutual repulsion with negatively or neutrally charged IB molecules.

Similar sorption patterns to IB are observed for STX. STX is significantly more adsorbed by LIG and BL 20:80, at 1.3 mg/g, compared to BEN at 0.01 mg/g. The pH_{eq} is 4.7 for LIG and 4.5 for BL 20:80. Under these pH conditions, the STX molecule is characterized by a neutral charge (Fig. 7). This leads to weak physical interaction with LIG and BL 20:80, primarily through hydrogen bonding and dispersion forces, and a repulsive interaction with negatively charged BEN at an pH_{eq} 9.3, where STX is also negatively charged.

In the case of SDBS, the highest adsorption occurs with LIG (4.60 mg/g) and BL 20:80 (4.70 mg/g) at pH_{eq} values of 6.2 for LIG and 6.8 for BL
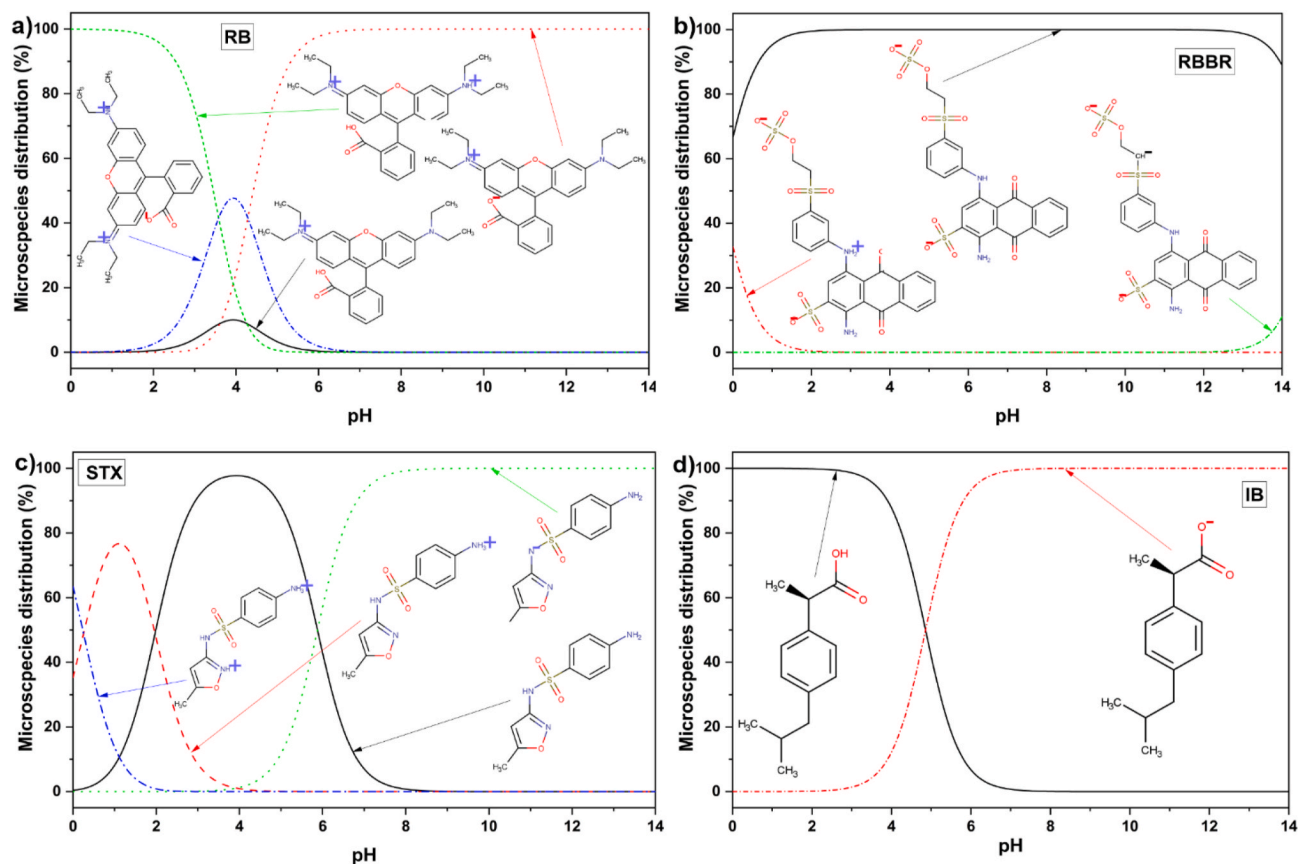
Fig. 7. Distribution forms of a) RB, b) RBBR, c) STX, d) IB as the function of different pH, based on modeling using *MarvinSketch* (ChemAxon, n.d.).

20:80, compared to 1.60 mg/g for BEN at a pH_{eq} 9 (Fig. 8). BEN becomes negatively charged at pH above 4.4 (its pH_{ZPC} value), repelling negatively charged SDBS molecules. A some small amount of SDBS may be adsorbed onto BEN through dispersion forces. Despite LIG and BL 20:80 being negatively charged at pH above 3.3, as indicated by their pH_{ZPC} results, these materials can still adsorb SDBS. The repulsion between SDBS molecules and the sorbents does not significantly impact the adsorption process. Several factors explain this: the hydrophobic properties of LIG, and to a lesser extent BL 20:80, enable hydrophobic interactions with SDBS molecules, which have relatively low polarity (65.58 Å²), the higher AEC of LIG and BL 20:80 compared to BEN increases their affinity for adsorbing SDBS anions, the presence of aliphatic groups and aromatic rings in SDBS's structure facilitates dispersion and π-π interaction with both adsorbents.

3.4. Post-sorption material characterization

Solid-state ^{13}C NMR characterization was conducted to examine the chemical state changes of RB, RBBR, STX, IB, and SDBS after sorption and their interactions with BL 20:80, LIG, and BEN. The sorption results for this experiment as well as FTIR studies of samples have been published elsewhere (Solińska et al., 2023); hence, our focus here is on describing the sorbent-sorbate interaction based on advanced NMR results. In most cases, the samples showed no signals from the sorbed organic molecules (indicating that the signals might be below the detection limits of the NMR method). The ^{13}C CP MAS NMR spectra of the samples after sorption of RBBR, IB, STX, and SDBS are presented in Figs. S3, S4, S5, and S6, respectively. Among these, only the BEN-STX showed weak signals from STX molecules in its spectrum (Fig. S5). The BEN-STX sample exhibits more signals in the aromatic region (100–150 ppm) compared to pure STX. This suggests physical interaction between BEN and STX's aromatic groups.

Fig. 9 displays the ^{13}C CP MAS NMR spectra of RB, the three tested sorbents, and samples after the adsorption of RB molecules. Characteristic signals for RB are observed in all samples after the sorption experiments. The ^{13}C MAS NMR spectra are identical across all types of sorption material used. They show minor changes compared to the parent material RB. Notably, there is a reduced number of signals in the samples post-sorption. Particularly, in the 90–120 ppm range, the number of signals from aromatic carbons decreased from six to three after the sorption. A similar observation was made for ibuprofen confined in the mesoporous material MCM-41, where a crystalline organic material exhibited 4 peaks from the aromatic ring. Still, after the sorption, there were only 2 signals in this region. This phenomenon was ascribed to increased mobility of the molecules, averaging the isotropic chemical shifts of aromatic carbons (Babonneau et al., 2004). Indeed, ^{13}C CP NMR spectra of RB in solution exhibit three signals from aromatic carbons in this range (Zheng et al., 2008). The carboxylic carbon signal appears at 164 ppm in the RB sample. The same signal is present in the spectra of the samples after sorption, but there is an additional signal after the sorption at 171 ppm. This down-field shifted signal could be due to carbon from the carboxylic group engaged in H-bonding (Jena et al., 2022).

3.5. Sorbents leaching study

Because there are no regulations concerning the permissible contents of elements that may be released into aqueous solutions from sorbents during their use, we compared the detected concentration of potentially environmentally risky elements released from composite BL 20:80 with the limitations attached to regulations and recommendations for the quality of drinking water proposed by the World Health Organization (World Health Organization, 2022), the U.S. Environmental Protection Agency (United States Environmental Protection Agency, n.d.), and the
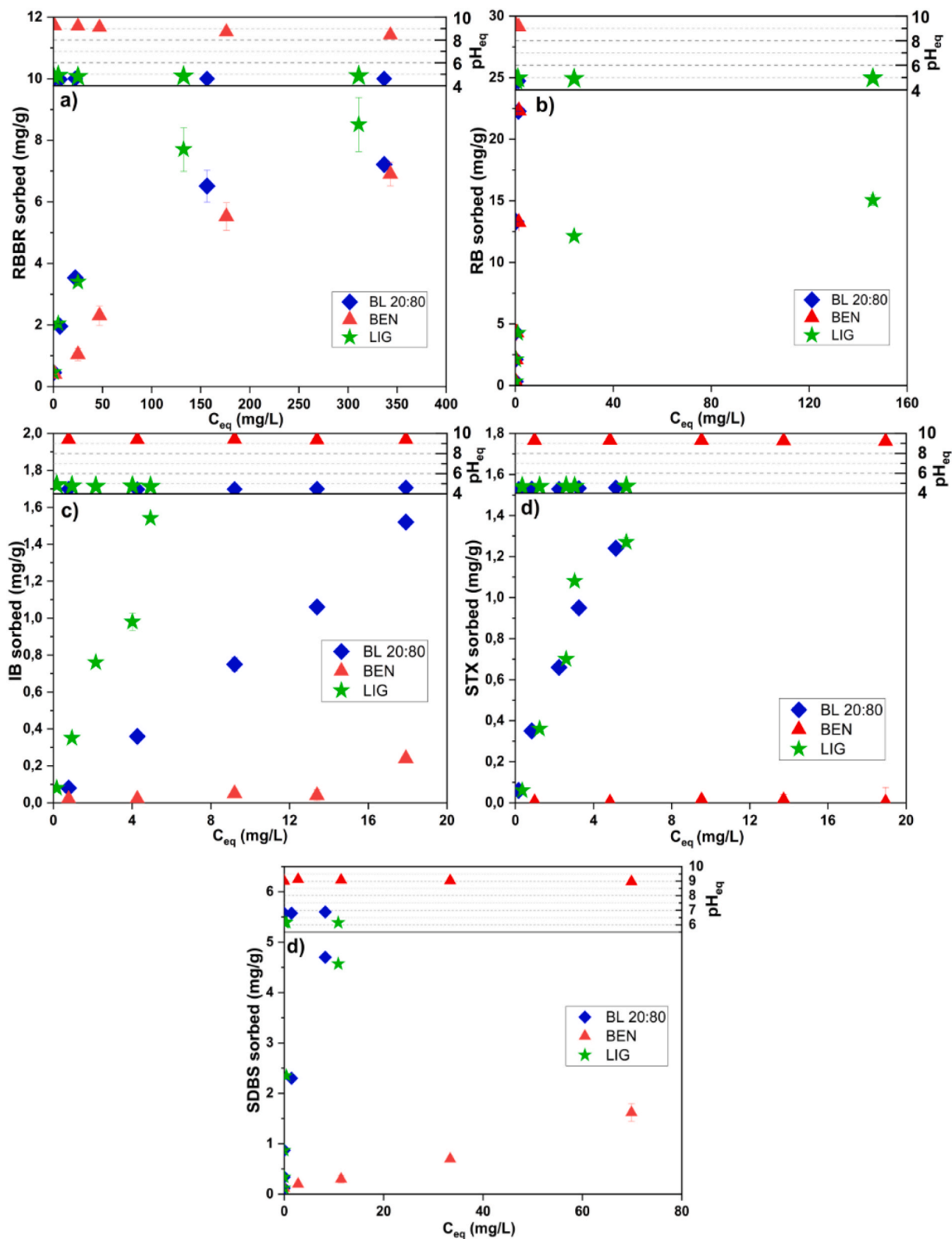
Fig. 8. The a) RBBR, b) RB, c) IB, d) STX, and e) SDBS sorption results on BEN, LIG, and BL 20:80 as the function of different C_{eq} of sorbates. The values above the sorption graphs indicate pH_{eq}.

European Parliament and the Council of the European Union (The European Parliament and the Council of the European Union, 2020), respectively. It appears that all detected elements leached from BL 20:80 do not exceed the concentration limits for drinking water presented in the documents cited above (Table 9). However, only the concentration

of Mn (0.06 mg/L) slightly exceeds the limitation proposed by the European Union (0.05 mg/L), but it meets the restriction proposed by the World Health Organization (0.1 mg/L). Nevertheless, our study reveals that mineral composite sorbent should not pose an environmental risk through secondary contaminations of purified water.
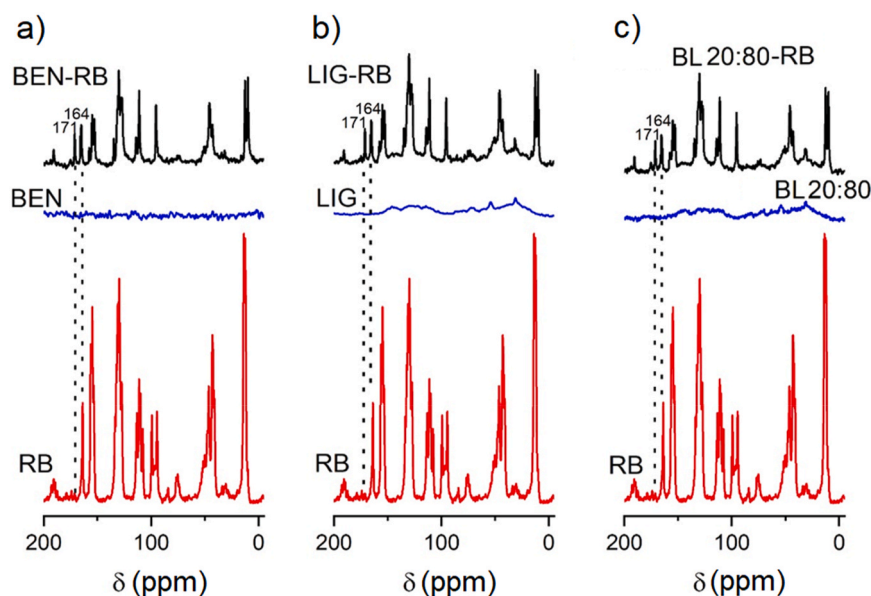
Fig. 9. ^{13}C CP MAS NMR spectra of samples after the sorption of RB on a) BEN, b) LIG, and c) BL 20:80. Dotted lines mark the signals from the carboxylic group.

Table 9
Results of sorbents leaching study.

Sample	Ag	Al	As	B	Ba	Be	Bi	Ca	Cd	Co
						[mg/L]				
LIG	b.d.	0.02	b.d.	0.15	0.05	b.d.	b.d.	65.50	b.d.	b.d.
BEN	b.d.	0.27	b.d.	b.d.	b.d.	b.d.	b.d.	6.06	b.d.	b.d.
BL 20:80	b.d.	b.d.	b.d.	0.11	0.03	b.d.	b.d.	43.73	b.d.	b.d.
	Cr	Cu	Fe	K	Li	Mg	Mn	Mo	Na	Ni
						[mg/L]				
LIG	b.d.	b.d.	0.02	0.95	b.d.	5.74	0.10	b.d.	1.37	b.d.
BEN	b.d.	b.d.	0.06	1.76	0.007	0.58	0.01	b.d.	9.06	b.d.
BL 20:80	b.d.	b.d.	0.01	1.61	b.d.	3.42	0.06	b.d.	3.14	b.d.
	P	Pb	SO_4^{2-}	Si	Sr	V	Zn	U	Hg	
						[mg/L]				
LIG	b.d.	b.d.	167.30	0.81	b.d.	b.d.	0.07	b.d.	0.001	
BEN	b.d.	b.d.	1.10	4.68	b.d.	b.d.	b.d.	b.d.	b.d.	
BL 20:80	b.d.	b.d.	96.60	1.46	b.d.	b.d.	0.02	b.d.	0.0003	

Abbreviations: b.d. - below detection limits [mg/L] for: Ag – 0.01; Al – 0.01; As – 0.1; B – 0.1; Ba – 0.01; Be – 0.005; Bi – 0.01; Cd – 0.01; Co – 0.01; Cr – 0.01; Cu – 0.005; Li – 0.005; Mo – 0.2; Ni – 0.05; P – 0.48; Pb – 0.01; Sr – 0.2; V – 0.05; Zn – 0.01; U – 0.0001; Hg – 0.0001.

Among the elements found in the LIG and BEN eluate, after reacting with redistilled water, that can be considered environmental problems are B, Ba, Mn, Li, Fe, SO_4^{2-}, Zn, and Hg. The leachable amount of B and Ba from LIG is below the concentration limit governed by regulations. A small amount of water-leachable Li is presented only in BEN and originates from ion-exchange positions in smectite minerals. Leachable Zn and Hg come from LIG, but some of their portions are uptaken by the BEN content in the BL 20:80 composite. As the results show, Zn in the composite is 0.02 mg/L (the calculated value is 0.06 mg/L) whereas Hg is 0.0003 mg/L (calculated to be 0.0008 mg/L). A similar situation is observed for Mn in the composite, where the expected concentration was calculated to be 0.08 mg/L, but the actual detected concentration is 0.06 mg/L. Fe released from LIG and BEN could have originated from Fe-containing admixtures; the amount of leached Fe is higher for BEN than LIG. Again, in BL 20:80, the concentration of Fe is smaller than expected (0.01 whereas calculated as 0.03 mg/L). Here, the formation of some Fe complex with the organic matter of LIG might be responsible for its immobilization (Baruah et al., 1981). Generally, after the water-leaching procedure, the chemical composition of the solutions shows that mainly the elements that are part of the sorbent-building minerals are leached from the sorbent samples, e.g., Ca, Na, K, Al, Si, and SO_4^{2-}. SO_4^{2-} is leached mainly from LIG (167.3 mg/L), to a lesser extent from BL 20:80 (96.60 mg/L), and least from BEN (1.10 mg/L). The source of released SO_4^{2-} from LIG is associated with the presence of S-content admixtures like pyrite (by S^{2-} oxidation) (Usher et al., 2004) and gypsum (Fig. 1) and also could be related to organically bound sulfur in matter built of such coals (Fleig et al., 2009). Ca comes from the calcite and gypsum in the LIG and the ion-exchange position in smectite minerals in BEN. In addition, noteworthy is the presence of Mg, leaching from LIG, and Na, K occurring at the ion-exchange positions of montmorillonite, the main component of the BEN sample. Al and Si should be associated with the reaction of clay minerals in all samples, mainly BEN.

3.6. Sorption from real wastewater from a municipal wastewater treatment plant

All conducted experiments supported the determination and characterization of BL 20:80's properties as a sorbent for the practical removal of organic compounds, such as dyes, pharmaceuticals, and surfactants, from contaminated water. Consequently, the BL 20:80 composite was used in an experiment to assess its the effect on the real wastewater from a municipal wastewater treatment plant in the southern part of Poland (Table 4), which was mixed with RB, RBBR, IB, STX, and SDBS at concentrations of 50 mg/L (RB, RBBR) and 10 mg/L (IB,

STX, SDBS), respectively. Fig. 10 presents the sorbate removal efficiencies resulting from three different adsorbent dosages: 1, 5, and 10 g/L. In general, a higher sorbent dosage results in greater removal efficiency for all sorbed organic compounds. This is associated with an increase in sorption active sites on the material's surface due to the increased amount of sorbent. The highest removal efficiency from wastewater, up to 98%, was observed for RB at the dosage of 10 g/L. The

second dye, RBBR, showed removal efficiencies of up to 58%, increasing with the solid-to-wastewater ratio. For pharmaceuticals, this ratio reached up to 25% for STX and 26% for IB. The surfactant SDBS showed removal efficiencies of up to 88% at a dosage 10 g/L. The variation in sorption efficiency, influenced by several factors, including the competitive effect of sorbate sorption, the chemical variation of the sorbed organic compounds, and the solution's pH. The initial pH of the
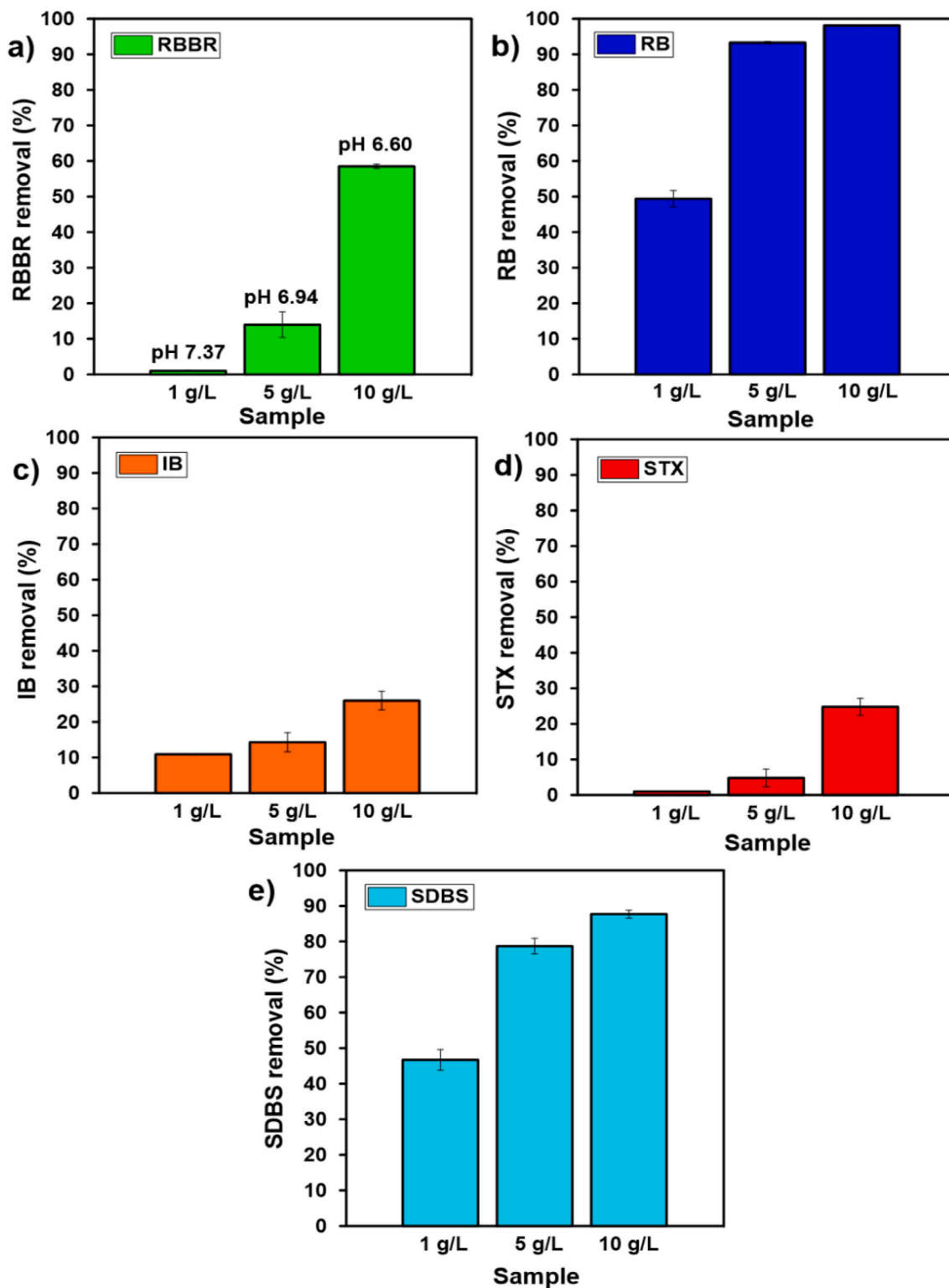

Fig. 10. The sorption efficiency of a) RBBR, b) RB, c) IB, d) STX, and e) SDBS from real wastewatercollected from municipal wastewater treatment planton BL 20:80. The values above the sorption graphs indicate pH_{eq}.

wastewater, containing five sorbed organic compounds, was 8.1. After sorption onto BL 20:80, at dosage 1, 5, and 10 g/L, the pH_{eq} solutions were 7.4, 6.9, and 6.6, respectively. The decrease in pH value, with an increasing amount of sorbent, is attributed to the acidic nature of the composite, dominated by LIG. At pH > 3.3, BL 20:80 becomes negatively charged; as a result, it most effectively sorbs the cationic forms of the sorbates. Unlike the others, RB does not form anionic forms at such a pH value, instead existing in the solution predominantly as zwitterion (RB ±). The remaining compounds are in anionic form (Fig. 7), which explains their lower sorption efficiency, with the exception of SDBS. However, as the pH decreases with an increased dosage of sorbent, the number of negative charges on the sorbent's surface decreases. Consequently, the sorption efficiency of the anionic forms of RBBR, STX, IB, and SDBS increases. The adsorption on anionic forms of the tested organic compounds tested is also facilitated by the composite's hydrophobic features, which promote hydrophobic interactions with organic molecules, while its AEC property enhances anionic exchange sorption behavior. Of note is the relatively high sorption efficiency of SDBS. This may be attributed to the steric effects on RBBR, STX, and IB molecules, whose geometry could obstruct the access of their functional groups in the matrix solution to interact with the sorption-active surface of the composite, unlike SDBS molecules. The sorption competition effect, involving the anionic/cationic forms of elements from wastewater (Table 4), along with the simultaneous presence of RB, RBBR, STX, IB, and SDBS in matrix solution, will also influence the amount of each tested organic compound adsorbed. The presence of various functional groups in each dye, pharmaceutical, and surfactant may enhance electrostatic interactions, van der Waals forces, and/or hydrogen bond formation between these organic compounds, influencing the amount adsorbed on the composite's surface. The presence of anionic/cationic forms of elements in wastewater could lead to decreased adsorption of RB, RBBR, STX, IB, and SDBS due competition for active sorption sites on the composite's surface.

4. Conclusion

The study thoroughly evaluated the bentonite-lignite composite (BL 20:80) for removing organic compounds such as dyes (Rhodamine B, Remazol Brilliant Blue R), pharmaceuticals (ibuprofen, sulfamethoxazole), and the surfactant sodium dodecylbenzenesulfonate from water. This set of experiments provided valuable data on the behavior of the used mineral composite and the influence of each component, BEN and LIG. The BL 20:80 composite, with 80 wt% lignite, demonstrated superior sorption performance due to the combination of the high surface area and porosity of BEN and the functional groups and hydrophobic properties of LIG The BL 20:80 composite achieved a maximum sorption of RB, RBBR, IB, STX, and SDBS equaled to 22.8 mg/g, 18.9 mg/g, 1.77 mg/g, 1.47 mg/g, and 4.70 mg/g, respectively. The leaching tests indicated that the BL 20:80 composite did not release hazardous levels of elements, ensuring no secondary contamination of purified water. The real wastewater experiments confirmed that composite could effectively remove RB (up to 98%), RBBR (58%), IB (26%), STX (25%), and SDBS (88%). These results suggest that the BL 20:80 composite is a viable sorbent for wastewater treatment, capable of effectively removing a variety of organic pollutants. Future studies will explore the granulated BL 20:80 composite and its usability in dynamic column systems, following the design of purification technologies.

CRediT authorship contribution statement

Agnieszka Solińska: Writing – review & editing, Writing – original draft, Visualization, Validation, Supervision, Project administration, Methodology, Investigation, Funding acquisition, Formal analysis, Data curation, Conceptualization. **Tomasz Bajda:** Writing – review & editing, Writing – original draft, Visualization, Formal analysis. **Mariusz Gackowski:** Writing – review & editing, Writing – original draft, Visualization, Formal analysis, Data curation.

Declaration of competing interest

The authors declare that they have no known competing financial interests or personal relationships that could have appeared to influence the work reported in this paper.

Data availability

Data will be made available on request.

Acknowledgement

Appendix A. Supplementary data

Supplementary data to this article can be found online at https://doi.org/10.1016/j.jclepro.2024.143555.

References

Akhtar, J., Amin, N.A.S., Shahzad, K., 2016. A review on removal of pharmaceuticals from water by adsorption. Desalination Water Treat. 57 https://doi.org/10.1080/19443994.2015.1051121.

Amirianshoja, T., Junin, R., Kamal Idris, A., Rahmani, O., 2013. A comparative study of surfactant adsorption by clay minerals. J. Petrol. Sci. Eng. 101 https://doi.org/10.1016/j.petrol.2012.10.002.

Ammar, M., Yousef, E., Mahmoud, M.A., Ashraf, S., Baltrusaitis, J., 2023. A comprehensive review of the developments in electrocoagulation for the removal of contaminants from wastewater. Separations 10. https://doi.org/10.3390/separations10060337.

Anliker, S., Patrick, M., Fenner, K., Singer, H., 2020. Quantification of active ingredient losses from formulating pharmaceutical industries and contribution to wastewater treatment plant emissions. Environ. Sci. Technol. 54 https://doi.org/10.1021/acs.est.0c05178.

APHA [American Public Health Association], 1999. Standard Methods for the Examination of Water and Wastewater (Twentieth Edition). American Public Health Association.

Arora, J., Ranjan, A., Chauhan, A., Biswas, R., Rajput, V.D., Sushkova, S., Mandzhieva, S., Minkina, T., Jindal, T., 2022. Surfactant pollution, an emerging threat to ecosystem: approaches for effective bacterial degradation. J. Appl. Microbiol. 133, 1229–1244. https://doi.org/10.1111/jam.15631.

Avisar, D., Primor, O., Gozlan, I., Mamane, H., 2010. Sorption of sulfonamides and tetracyclines to montmorillonite clay. Water Air Soil Pollut. 209, 439–450. https://doi.org/10.1007/s11270-009-0212-8.

Babonneau, F., Yeung, L., Steunou, N., Gervais, C., Ramila, A., Vallet-Regi, M., 2004. Solid state NMR characterisation of encapsulated molecules in mesoporous silica. J. Sol. Gel Sci. Technol. 31, 219–223. https://doi.org/10.1023/B:JSST.0000047991.73840.8b.

Badmus, S.O., Amusa, H.K., Oyehan, T.A., Saleh, T.A., 2021. Environmental risks and toxicity of surfactants: overview of analysis, assessment, and remediation techniques. Environ. Sci. Pollut. Control Ser. 28, 62085–62104. https://doi.org/10.1007/s11356-021-16483-w.

Barrett, E.P., Joyner, L.G., Halenda, P.P., 1951. The determination of pore volume and area distributions in porous substances. I. Computations from nitrogen isotherms. J. Am. Chem. Soc. 73 https://doi.org/10.1021/ja01145a126.

Baruah, M.K., Upreti, M.C., Baishya, N.K., Dutta, S.N., 1981. Interaction of iron with humic acid extracted from lignite. Fuel 60. https://doi.org/10.1016/0016-2361(81)90094-6.

Belete, B., Desye, B., Ambelu, A., Yenew, C., 2023. Micropollutant removal efficiency of advanced wastewater treatment plants: a systematic review. Environ. Health Insights 17. https://doi.org/10.1177/11786302231195158.

Berhane, T.M., Levy, J., Krekeler, M.P.S., Danielson, N.D., 2017. Kinetic sorption of contaminants of emerging concern by a palygorskite-montmorillonite filter medium. Chemosphere 176, 231–242. https://doi.org/10.1016/j.chemosphere.2017.02.068.

Breen, C., Madejová, J., Komadel, P., 1995. Characterisation of moderately acid-treated, size-fractionated montmorillonites using IR and MAS NMR spectroscopy and thermal analysis. J. Mater. Chem. 5 https://doi.org/10.1039/JM9950500469.

Brunauer, S., Emmett, P.H., Teller, E., 1938. Adsorption of gases in multimolecular layers. J. Am. Chem. Soc. 60 https://doi.org/10.1021/ja01269a023.

Burzio, C., Ekholm, J., Modin, O., Falås, P., Svahn, O., Persson, F., van Erp, T., Gustavsson, D.J.I., Wilén, B.M., 2022. Removal of organic micropollutants from municipal wastewater by aerobic granular sludge and conventional activated sludge. J. Hazard Mater. 438 https://doi.org/10.1016/j.jhazmat.2022.129528.

ChemAxon, n.d. MarvinSketch [WWW Document]. URL https://chemaxon.com.

Clara, M., Gans, O., Windhofer, G., Krenn, U., Hartl, W., Braun, K., Scharf, S., Scheffknecht, C., 2011. Occurrence of polycyclic musks in wastewater and receiving water bodies and fate during wastewater treatment. Chemosphere 82. https://doi.org/10.1016/j.chemosphere.2010.11.041.

Debamita, C., Rampal, N., Gautham, J.P., Vairavel, P., 2020. Process optimization, isotherm, kinetics, and thermodynamic studies for removal of remazol brilliant blue-r dye from contaminated water using adsorption on guava leaf powder. Desalination Water Treat. 185, 318–343. https://doi.org/10.5004/dwt.2020.25395.

Devaisy, S., Kandasamy, J., Aryal, R., Johir, M.A.H., Ratnaweera, H., Vigneswaran, S., 2023. Removal of organics with ion-exchange resins (IEX) from reverse osmosis concentrate. Membranes 13. https://doi.org/10.3390/membranes13020136.

Dikmen, S., Ersoy, B., Dikmen, Z., 2020. Adsorption behaviour of ionic and non-ionic surfactants onto talc a naturally hydrophobic mineral-a comparative study. Eskisehir Technical University Journal of Science and Technology A - Applied Sciences and Engineering 21, 139–152. https://doi.org/10.18038/estubtda.829712.

Donkadokula, N.Y., Kola, A.K., Naz, I., Saroj, D., 2020. A review on advanced physico-chemical and biological textile dye wastewater treatment techniques. Rev. Environ. Sci. Biotechnol. 19, 543–560. https://doi.org/10.1007/s11157-020-09543-z.

Dubinin, M.M., 1960. The potential theory of adsorption of gases and vapors for adsorbents with energetically nonuniform surfaces. Chem. Rev. 60, 235–241. https://doi.org/10.1021/cr60204a006.

Eftekhari, S., Habibi-Yangjeh, A., Sohrabnezhad, S.H., 2010. Application of AlMCM-41 for competitive adsorption of methylene blue and rhodamine B: thermodynamic and kinetic studies. J. Hazard Mater. 178, 349–355. https://doi.org/10.1016/j.jhazmat.2010.01.086.

Ehsan, A., Bhatti, H.N., Iqbal, M., Noreen, S., 2017. Native, acidic pre-treated and composite clay efficiency for the adsorption of dicationic dye in aqueous medium. Water Sci. Technol. 75 https://doi.org/10.2166/wst.2016.435.

Ewis, D., Ba-Abbad, M.M., Benamor, A., El-Naas, M.H., 2022. Adsorption of organic water pollutants by clays and clay minerals composites: a comprehensive review. Appl. Clay Sci. 229 https://doi.org/10.1016/j.clay.2022.106686.

Fleig, D., Normann, F., Andersson, K., Johnsson, F., Leckner, B., 2009. The fate of sulphur during oxy-fuel combustion of lignite. Energy Proc. 1, 383–390. https://doi.org/10.1016/j.egypro.2009.01.052.

Gil, A., Santamaría, J., Korili, S.A., Vicente, M.A., Barbosa, L.V., de Souza, S.D., Marçal, L., de Faria, E.H., Ciuffi, K.J., 2021. A review of organic-inorganic hybrid clay based adsorbents for contaminants removal: synthesis, perspectives and applications. J. Environ. Chem. Eng. 9 https://doi.org/10.1016/j.jece.2021.105808.

Hai, F.I., Price, W.E., 2021. Removal of pharmaceuticals from wastewater by membrane bioreactors: factors, mechanisms, and perspectives. Handb. Environ. Chem. 108, 223–238. https://doi.org/10.1007/698_2020_676.

He, Q., Ruan, P., Miao, Z., Wan, K., Gao, M., Li, X., Huang, S., 2021. Adsorption of direct yellow brown D3G from aqueous solution using loaded modified low-cost lignite: performance and mechanism. Environ. Technol. 42, 1642–1651. https://doi.org/10.1080/09593330.2019.1675774.

Henc, M., Tomaszewicz, M., Tsuboi, Y., Sawicki, J., Tomaszewicz, G., Zuwała, J., 2018. In: Use Lignite in Gasification—Review of Polish Wroclaw - Japan Project „UCESP'' [WWW Document]. DRYLING Project Final Workshop: Competitive Pre-drying Technologies and Firing Concepts for Flexible and Efficient Lignite Utilization.

Ighalo, J.O., Yap, P.S., Iwuozor, K.O., Aniagor, C.O., Liu, T., Dulta, K., Iwuchukwu, F.U., Rangabhashiyam, S., 2022. Adsorption of persistent organic pollutants (POPs) from the aqueous environment by nano-adsorbents: a review. Environ. Res. 212 https://doi.org/10.1016/j.envres.2022.113123.

Isik, O., Erbil, M.C., Abdelrahman, A.M., Ersahin, M.E., Koyuncu, I., Ozgun, H., Demir, I., 2022. Removal of micropollutants from municipal wastewater by membrane bioreactors: conventional membrane versus dynamic membrane. J. Environ. Manag. 303 https://doi.org/10.1016/j.jenvman.2021.114233.

Janusz, W., 1994. Electrical double layer at the metal oxide/electrolyte interface in interfacial forces and fields. Theory and Applications in Surfactant Science. Marcel Dekker, New York chap. 4.

Jena, S., Routray, C., Dutta, J., Biswal, H.S., 2022. Hydrogen bonding directed reversal of 13C NMR chemical shielding. Angew. Chem. Int. Ed. https://doi.org/10.1002/anie.202207521.

Johnson, J.L., Dodder, N.G., Mladenov, N., Steinberg, L., Richardot, W.H., Hoh, E., 2024. Comparison of trace organic chemical removal efficiencies between aerobic and anaerobic membrane bioreactors treating municipal wastewater. ACS ES and T Water 4, 1381–1392. https://doi.org/10.1021/acsestwater.3c00542.

Johnson, P., Trybala, A., Starov, V., Pinfield, V.J., 2021. Effect of synthetic surfactants on the environment and the potential for substitution by biosurfactants. Adv. Colloid Interface Sci. 288 https://doi.org/10.1016/j.cis.2020.102340.

Jones, E.R., Van Vliet, M.T.H., Qadir, M., Bierkens, M.F.P., 2021. Country-level and gridded estimates of wastewater production, collection, treatment and reuse. Earth Syst. Sci. Data 13. https://doi.org/10.5194/essd-13-237-2021.

Karić, N., Maia, A.S., Teodorović, A., Atanasova, N., Langergraber, G., Crini, G., Ribeiro, A.R.L., Đolić, M., 2022. Bio-waste valorisation: agricultural wastes as biosorbents for removal of (in)organic pollutants in wastewater treatment. Chemical Engineering Journal Advances 9. https://doi.org/10.1016/j.ceja.2021.100239.

Katare, A.K., Tabassum, A., Sharma, A.K., Sharma, S., 2023. Treatment of pharmaceutical wastewater through activated sludge process—a critical review. Environ. Monit. Assess. 195 https://doi.org/10.1007/s10661-023-11967-3.

Kausar, A., Iqbal, M., Javed, A., Aftab, K., Nazli, Z.i.H., Bhatti, H.N., Nouren, S., 2018. Dyes adsorption using clay and modified clay: a review. J. Mol. Liq. 256 https://doi.org/10.1016/j.molliq.2018.02.034.

Kietzmann, M., 1993. Reviews of environmental contamination and toxicology. Toxicon. https://doi.org/10.1016/0041-0101(93)90366-q.

Klamerth, N., Malato, S., Agüera, A., Fernández-Alba, A., Mailhot, G., 2012. Treatment of municipal wastewater treatment plant effluents with modified photo-fenton as a tertiary treatment for the degradation of micro pollutants and disinfection. Environ. Sci. Technol. 46 https://doi.org/10.1021/es204112d.

Kumar, R., Sarmah, A.K., Padhye, L.P., 2019. Fate of pharmaceuticals and personal care products in a wastewater treatment plant with parallel secondary wastewater treatment train. J. Environ. Manag. 233, 649–659. https://doi.org/10.1016/j.jenvman.2018.12.062.

Lan, D., Zhu, H., Zhang, J., Li, S., Chen, Q., Wang, C., Wu, T., Xu, M., 2022. Adsorptive removal of organic dyes via porous materials for wastewater treatment in recent decades: a review on species, mechanisms and perspectives. Chemosphere 293. https://doi.org/10.1016/j.chemosphere.2021.133464.

Li, Y., Wei, M., 2022. Evaluation on adsorption capacity of low organic matter soil for hydrophobic organic pollutant. J. Environ. Chem. Eng. 10 https://doi.org/10.1016/j.jece.2022.107561.

Linclau, E., Ceulemans, J., De Sitter, K., Cauwenberg, P., 2016. Water and detergent recovery from rinsing water in an industrial environment. Water Resour. Ind. 14, 3–10. https://doi.org/10.1016/j.wri.2016.03.001.

Madejová, J., Bujdák, J., Gates, W.P., Komadel, P., 1996. Preparation and infrared spectroscopic characterization of reduced-charge montmorillonite with various Li contents. Clay Miner. 31 https://doi.org/10.1180/claymin.1996.031.2.09.

Mansouri, F., Chouchene, K., Roche, N., Ksibi, M., 2021. Removal of pharmaceuticals from water by adsorption and advanced oxidation processes: state of the art and trends. Appl. Sci. 11 https://doi.org/10.3390/app11146659.

Mantovani, M., Rossi, S., Ficara, E., Collina, E., Marazzi, F., Lasagni, M., Mezzanotte, V., 2024. Removal of pharmaceutical compounds from the liquid phase of anaerobic sludge in a pilot-scale high-rate algae-bacteria pond. Sci. Total Environ. 908 https://doi.org/10.1016/j.scitotenv.2023.167881.

Mao, Y., Zhao, Y., Cotterill, S., 2023. Examining current and future applications of electrocoagulation in wastewater treatment. Water (Switzerland) 15. https://doi.org/10.3390/w15081455.

Moretti, A., Ivan, H.L., Skvaril, J., 2024. A review of the state-of-the-art wastewater quality characterization and measurement technologies. Is the shift to real-time monitoring nowadays feasible? J. Water Proc. Eng. 60 https://doi.org/10.1016/j.jwpe.2024.105061.

Palmer, M., Hatley, H., 2018. The role of surfactants in wastewater treatment: impact, removal and future techniques: a critical review. Water Res. 147, 60–72. https://doi.org/10.1016/j.watres.2018.09.039.

Pathak, N., Tran, V.H., Merenda, A., Johir, M.A.H, Phuntsho, S., Shon, H., 2020. Removal of organic micro-pollutants by conventional membrane bioreactors and high-retention membrane bioreactors. Appl. Sci. 10 https://doi.org/10.3390/APP10082969.

Pedretti, A., Mazzolari, A., Gervasoni, S., Fumagalli, L., Vistoli, G., 2021. The VEGA suite of programs: an versatile platform for cheminformatics and drug design projects. Bioinformatics 37. https://doi.org/10.1093/bioinformatics/btaa774.

Perkins, E.J., Habib, T., Escalon, B.L., Cavallin, J.E., Thomas, L., Weberg, M., Hughes, M. N., Jensen, K.M., Kahl, M.D., Villeneuve, D.L., Ankley, G.T., Garcia-Reyero, N., 2017. Prioritization of contaminants of emerging concern in wastewater treatment plant discharges using chemical:gene interactions in caged fish. Environ. Sci. Technol. 51 https://doi.org/10.1021/acs.est.7b01567.

Rezazadeh, N., Danesh, S., Eftekhari, M., 2023. Investigation the adsorption mechanism of a non-ionic surfactant on graphene oxide and its derivatives (kinetic, isotherm curves, thermodynamic, and effect of salts studies). Environ. Nanotechnol. Monit. Manag. 20 https://doi.org/10.1016/j.enmm.2023.100819.

Rozalén, M., Brady, P.V., Huertas, F.J., 2009. Surface chemistry of K-montmorillonite: ionic strength, temperature dependence and dissolution kinetics. J. Colloid Interface Sci. 333 https://doi.org/10.1016/j.jcis.2009.01.059.

Santos, D.H.S., Santos, J.P.T.S., Duarte, J.L.S., Oliveira, L.M.T.M., Tonholo, J., Meili, L., Zanta, C.L.P.S., 2022. Regeneration of activated carbon adsorbent by anodic and cathodic electrochemical process. Process Saf. Environ. Protect. 159 https://doi.org/10.1016/j.psep.2022.01.083.

Shakir, K., Elkafrawy, A.F., Ghoneimy, H.F., Elrab Beheir, S.G., Refaat, M., 2010. Removal of rhodamine B (a basic dye) and thoron (an acidic dye) from dilute aqueous solutions and wastewater simulants by ion flotation. Water Res. 44, 1449–1461. https://doi.org/10.1016/j.watres.2009.10.029.

Shreya, Verma, A.K., Dash, A.K., Bhunia, P., Dash, R.R., 2021. Removal of surfactants in greywater using low-cost natural adsorbents: a review. Surface. Interfac. 27 https://doi.org/10.1016/j.surfin.2021.101532.

Sing, K., Everett, D., Haul, R., Moscou, L., Pierotti, R., Rouquerol, J., Siemieniewska, T., 1995. Reporting physisorption data for gas/solid systems with special reference to the determination of surface area and porosity (Recommendations 1984). Pure Appl. Chem. 57.

Solińska, A., Marchewka, J., Sitarz, M., Bajda, T., 2023. Infrared spectroscopy: the key to elucidating the sorption mechanism of surfactants, dyes and pharmaceuticals on mineral composite material. Spectrochim. Acta Mol. Biomol. Spectrosc. 299 https://doi.org/10.1016/j.saa.2023.122758.

Styszko, K., Nosek, K., Motak, M., Bester, K., 2015. Preliminary selection of clay minerals for the removal of pharmaceuticals, bisphenol A and triclosan in acidic and neutral aqueous solutions. Compt. Rendus Chem. 18, 1134–1142. https://doi.org/10.1016/j.crci.2015.05.015.

Tamanna, T., Mahon, P.J., Hockings, R.K., Alam, H., Raymond, M., Smith, C., Clarke, C., Yu, A., 2023. Ion exchange MIEX® GOLD resin as a promising sorbent for the removal of PFAS compounds. Appl. Sci. 13 https://doi.org/10.3390/app13106263.

The European Parliament and the Council of the European Union, 2020. Directive (EU) 2020/2184 of the European parliament and of the Council. Off. J. Eur. Union 2019, 1–62.

Thiele-Bruhn, S., Seibicke, T., Schulten, H.-R., Leinweber, P., 2004. Sorption of sulfonamide pharmaceutical antibiotics on whole soils and particle-size fractions. J. Environ. Qual. 33 https://doi.org/10.2134/jeq2004.1331.

Thompson, J.F., Morrison, G.R., 1951. Determination of organic nitrogen. Control of variables in the use of Nessler's reagent. Anal. Chem. 23 https://doi.org/10.1021/ac60056a029.

Tkac, I., Komadel, P., Muller, D., 1994. Acid-treated montmorillonites - a study by 29Si and 27Al MAS NMR. Clay Miner. 29.

United States Environmental Protection Agency. National Primary Drinking Water Regulations. n.d. https://www.epa.gov/ground-water-and-drinking-water/national-primary-drinking-water-regulations#Disinfectants.

Usher, C.R., Cleveland, C.A., Strongin, D.R., Schoonen, M.A., 2004. Origin of oxygen in sulfate during pyrite oxidation with water and dissolved oxygen: an in situ horizontal attenuated total reflectance infrared spectroscopy isotope study. Environ. Sci. Technol. 38, 5604–5606. https://doi.org/10.1021/es0494003.

Vasireddy, S., Morreale, B., Cugini, A., Song, C., Spivey, J.J., 2011. Clean liquid fuels from direct coal liquefaction: chemistry, catalysis, technological status and challenges. Energy Environ. Sci. https://doi.org/10.1039/c0ee00097c.

Vinayagam, V., Murugan, S., Kumaresan, R., Narayanan, M., Sillanpää, M., Viet N Vo, D., Kushwaha, O.S., Jenis, P., Potdar, P., Gadiya, S., 2022. Sustainable adsorbents for the removal of pharmaceuticals from wastewater: a review. Chemosphere 300. https://doi.org/10.1016/j.chemosphere.2022.134597.

Wang, J., He, Y., Ling, X., Hao, J., Xie, W., 2017. Adsorption performance of nonionic surfactant on the lignite particles with different density. Energy Fuel. 31, 6580–6586. https://doi.org/10.1021/acs.energyfuels.6b03087.

Wen, J., Yan, C., Xing, L., Wang, Q., Yuan, L., Hu, X., 2020. Simultaneous immobilization of as and Cd in a mining site soil using HDTMA-modified zeolite. Environ. Sci. Pollut. Control Ser. https://doi.org/10.1007/s11356-020-11477-6.

World Health Organization, 2022. Guidelines for Drinking-Water Quality: Fourth Edition Incorporating the First and Second Addenda. Geneva.

Wu, L., Du, C., He, J., Yang, Z., Li, H., 2020. Effective adsorption of diclofenac sodium from neutral aqueous solution by low-cost lignite activated cokes. J. Hazard Mater. 384, 121284 https://doi.org/10.1016/j.jhazmat.2019.121284.

Yalkowsky, R., Dannenfleser, S., 1992. Aquasol Database of Aqueous Solubility, fifth ed. College of Pharmacy. University of Arizona, Tucson, AZ.

Yuan, X., Lv, Z., Zhang, Z., Han, Y., Liu, Z., Zhang, H., 2023. A review of antibiotics, antibiotic resistant bacteria, and resistance genes in aquaculture: occurrence, contamination, and transmission. Toxics 11. https://doi.org/10.3390/toxics11050420.

Zawadzki, P., 2022. Visible light–driven advanced oxidation processes to remove emerging contaminants from water and wastewater: a review. In: Water, Air, and Soil Pollution. https://doi.org/10.1007/s11270-022-05831-2. Springer International Publishing.

Zhao, F., Mu, B., Zhang, T., Dong, C., Zhu, Y., Zong, L., Wang, A., 2023. Synthesis of biochar/clay mineral nanocomposites using oil shale semi-coke waste for removal of organic pollutants. Biochar 5, 1–21. https://doi.org/10.1007/s42773-023-00205-1.

Zheng, H., Shang, G.Q., Yang, S.Y., Gao, X., Xu, J.G., 2008. Fluorogenic and chromogenic rhodamine spirolactam based probe for nitric oxide by spiro ring opening reaction. Org. Lett. 10, 2357–2360. https://doi.org/10.1021/ol800206x.